NASA CONTRACTOR REPORT

NASA CR-2389

NASA CR-2389

USE OF MULTIPLE DISCRETE WALL JETS FOR DELAYING BOUNDARY LAYER SEPARATION

by J. D. McLean and H. J. Herring

Prepared by
PRINCETON UNIVERSITY
Princeton, N.J. 08540
for Lewis Research Center

NATIONAL AERONAUTICS AND SPACE ADMINISTRATION • WASHINGTON, D. C. • JUNE 1974

1. Report No.	2. Government Accession No.	3. Recipient's Catalog No.
NASA CR-2389		

4. Title and Subtitle	5. Report Date
USE OF MULTIPLE DISCRETE WALL JETS FOR DELAYING BOUNDARY LAYER SEPARATION	JUNE 1974
	6. Performing Organization Code

7. Author(s)	8. Performing Organization Report No.
J. D. McLean and H. J. Herring	None
	10. Work Unit No.

9. Performing Organization Name and Address	11. Contract or Grant No.
Princeton University James Forrestal Campus Princeton, New Jersey 08540	NGL 31-001-074
	13. Type of Report and Period Covered
12. Sponsoring Agency Name and Address	Contractor Report
National Aeronautics and Space Administration Washington D. C. 20546	14. Soonsoring Agency Code

15. Supplementary Notes

Final Report. Project Manager, Seymour Lieblein, V/STOL and Noise Division, NASA Lewis Research Center, Cleveland, Ohio

16. Abstract

The effectiveness of a spanwise array of small discrete blowing nozzles in preventing separation of a turbulent boundary layer was investigated experimentally. The spacing, axial location, and momentum flux of the nozzles were varied in a systematic way, and overall performance was measured for each combination. Extensive mean velocity profiles were measured for one selected combination. Overall diffusion achieved before separation was correlated successfully with a momentum flux excess parameter, and in terms of this parameter discrete nozzles, when advantageously placed, were found to perform somewhat better than an optimally placed two-dimensional jet slot.

17. Key Words (Suggested by Author(s))	18. Distribution Statement
Multiple wall jets; Boundary layer control, experimental; Turbulent boundary layer separation	Unclassified - unlimited Category 12

19. Security Classif. (of this report)	20. Security Classif. (of this page)	21. No. of Pages	22. Price*
Unclassified	Unclassified	74	$3.50

* For sale by the National Technical Information Service, Springfield, Virginia 22151

TABLE OF CONTENTS

NOTATION

A_j	cross-sectional area of a jet nozzle
d	jet nozzle diameter
E	local energy parameter (eq. (8))
E_o	system energy parameter
h	height of a two-dimensional jet slot
H	boundary layer shape factor, δ^*/θ
M	local momentum excess parameter (eq. (6))
M_o	system momentum excess parameter (eq. (9))
p	pressure
Q	local mass flux parameter (eq. (5))
Q_o	system mass flux parameter
S	spanwise nozzle spacing
u	velocity in the x direction
U	free-stream velocity
v	velocity in the y direction
x,y,z	Cartesian coordinates

Greek symbols

δ	boundary layer thickness
δ^*	displacement thickness
δ^{**}	energy thickness
ρ	density
τ	shear stress
θ	momentum thickness
Θ	modified momentum thickness (eq. (4))

Subscripts

j	at the nozzle exit
o	at the beginning of the pressure gradient. Taken to be the station where the attempted linear velocity distribution intersects $U/U_{max} = 1$ (see Fig. 16). Generally not x=0
max	maximum value at the high speed section of tunnel
∞	at the edge of the boundary layer
s	at separation
so	at separation without jets (assuming the same pressure distribution)

INTRODUCTION

Boundary layer separation occurs in any situation where a boundary layer flow is subjected to a positive pressure gradient (pressure increasing in the streamwise direction) over a sufficient streamwise distance. The effect of the pressure gradient is to retard the lower velocity fluid near the wall until the shear stress at the wall, which is proportional to the velocity gradient at the wall, has decreased to zero. At this point the boundary layer is said to be separated, and downstream of this point a region of re-circulating "dead air" is formed adjacent to the wall. The region downstream of separation cannot support a strong pressure gradient, and, as a result, only a very small additional pressure increase can generally occur after separation. This effect occurs whether the flow is external (as in the case of a wing) or internal (as in the case of a diffuser). In practical applications, separation, with its attendant prevention of further pressure increase, is usually detrimental to the performance of fluid flow devices.

One widely used method of delaying separation, and thereby increasing the possible pressure rise, is to produce a wall jet by forcing fluid through a tangential blowing slot in the wall. The high velocity fluid injected through the slot mixes with and re-energizes the retarded fluid near the wall, enabling the boundary layer to negotiate the adverse pressure gradient for a greater distance downstream. If the momentum added by the jet is sufficient, separation can be prevented until the free-stream has nearly stagnated, and a pressure recovery factor near unity can be achieved.

The object of the work reported here is to investigate the possibility of replacing the jet slot with a spanwise array of discrete, round nozzles, which would discharge fluid in the streamwise direction parallel to the wall surface. These nozzles could be placed with one edge flush with the wall surface, or they could be displaced a small distance away from the wall surface. Such an array of nozzles introduces a basic three-dimensionality which distinguishes discrete jet flow from the wall jet flow produced by a slot. Only asymptotically in the far field would the flow produced by discrete nozzles be expected to approach the flow produced by a slot. The three-dimensionality of the discrete jet flow field produces some interesting effects. A companion report [1] explores some of these effects in the case of discrete jets issuing into still air adjacent to a flat wall. The present report deals with discrete jets issuing into a co-flowing stream, particularly a co-flowing stream in which separation would normally occur.

At the outset, two definite advantages over the use of slots were considered to justify a study of the use of discrete jets:

1) Discrete jet nozzles and their associated ducting are simpler to construct than slots, especially in the case of high supply pressures.

2) Discrete jets are easier to incorporate into surrounding structures.

These advantages were probably the deciding factors in the only case known to the authors where discrete jets have been used in a practical application. In that case, discrete jets were used to form an internal ejector pump running the full span of a suction-blowing wing flap in flight tests performed by O.N.E.R.A. (Ref. [2], pp. 35-39).

Given the practical structural advantages of discrete jet installations, the purpose of the work reported here is to explore the fluid dynamic preformance of discrete jets in comparison with the performance of slot jets. Since slots are difficult to construct to a sufficiently high standard for definitive experimental work, time did not permit inclusion of a two-dimensional jet flow in the experimental program reported here. It was necessary, therefore, to rely on the data of other investigators for comparisons with two-dimensional flows.

Two-dimensional wall jets, with and without external streams, have been studied extensively. Refs. [3] and [4] are surveys which provide an over-view of the voluminous body of research which has been devoted to the study of wall jets. But in general, cases with separation have received less attention than the more easily studied cases of quiescent air and constant free-stream velocity. Early investigations into cases with separation tended to be of an applied nature, stressing the overall performance of wing flaps with blowing slots. Many such investigations are reported in Ref. [2], but because they generally do not include detailed boundary layer measurements, these results are of little use in the development of modern prediction methods. More recently, McGahan [5] has made extensive, systematic measurements of mean velocity profiles in a separating flow with a blowing slot which was placed sequentially in several different axial locations in the flow. To the authors' knowledge, McGahan has made the only sufficiently detailed measurements of a separating flow to provide a direct comparison with the discrete jet data to be reported here.

An exploratory study of discrete jets faces a basic difficulty in that there are more geometric variables to be dealt with than there are in the case of two-dimensional jets. The nozzle diameter and the spanwise spacing between nozzles can, of course, be varied independently. In combination, they determine the nozzle cross-sectional area per unit span, which is the discrete jet equivalent of the two-dimensional slot height. In addition, the height of the nozzle axes above the wall is an available variable because discrete nozzles, unlike slots, can be placed at some distance from the wall surface without causing a great deal of drag. When these geometric variables are combined with the usual jet variables (mass, momentum, and energy fluxes), it can be seen that the parameter space to be explored in a study of this type is large indeed. For this reason, the program of experimental research to be described in this report was designed to be carried out in two distinct phases. In the first phase, many different flow geometries were set up in the wind tunnel, covering as much of the geometric parameter space as was practical. Because of the large number of cases, only the overall performance of the jets, in terms of the pressure recovery of the external flow, was measured in each case. On the basis of this exploratory phase of the study, one particular flow was chosen for detailed flow field measurements. The apparatus and the experimental program are discussed in detail in the following sections.

ANALYTICAL BACKGROUND

In interpreting the performance of both discrete and two-dimensional wall jets, it is helpful to use dimensionless parameters which arise naturally from the equations of motion. In deriving these parameters, we will consider a flow which is planar, two-dimensional, and steady past a smooth, flat wall with a slot jet. To cover the case of discrete jets, an analogous derivation can be given in three dimensions, and the resulting parameters are equivalent to those derived below. Since the final results are the same, only the simpler two-dimensional derivation will be given here. The effects of viscosity and turbulence will be restricted to a layer of thickness δ, as shown in Fig. 1. We further restrict our attention to external streams of low Mach number, where the density outside the boundary layer can be considered constant. To allow for the possibility of high velocity jet flows, however, the density will be considered variable within the boundary layer. In the notation of Schlichting [6], the momentum and continuity equations can be written:

$$\rho u \frac{\partial u}{\partial x} + \rho v \frac{\partial u}{\partial y} + \frac{\partial P}{\partial x} = \frac{\partial \tau_{xy}}{\partial y} + \frac{\partial \tau_{xx}}{\partial x} \tag{1}$$

$$\frac{\partial (\rho u)}{\partial x} + \frac{\partial (\rho v)}{\partial y} = 0 \tag{2}$$

Note that none of the usual boundary layer assumptions have been made. With the assumption of constant free-stream density and the use of Bernouli's equation, eq. (1) can be re-written:

$$\rho u \frac{\partial u}{\partial x} + \rho v \frac{\partial u}{\partial y} - \rho_\infty U \frac{dU}{dx} + \frac{\partial}{\partial x}(P - P_\infty) = \frac{\partial \tau_{xy}}{\partial y} + \frac{\partial \tau_{xx}}{\partial x} \quad , \tag{3}$$

where the pressure is still allowed to vary within the boundary layer. Integrating eq. (3) from the wall in the y direction, we obtain:

$$\rho_\infty U \frac{dU}{dx} \delta^* + \frac{d}{dx}(\rho_\infty U^2 \Theta) = \tau_w + \int_0^\delta \frac{\partial \tau_{xx}}{\partial x} dy \tag{4}$$

where

$$\delta^* = \int_0^\delta \left(1 - \frac{\rho u}{\rho_\infty U}\right) dy$$

$$\Theta = \int_0^\delta \left[\frac{\rho u}{\rho_\infty U}\left(1 - \frac{u}{U}\right) + \frac{P - P_\infty}{\rho_\infty U^2}\right] dy$$

Everywhere except in the immediate vicinity of the slot, the pressure will be nearly constant with y, and $\partial \tau_{xx}/\partial x$ will be negligible, in which case eq. (4) reduces to the usual integral momentum equation for a boundary layer, and Θ becomes the usual momentum thickness.

At the location of the jet, δ^* and Θ are not continuous. The derivative in the second term of eq. (4) ceases to exist at the jet exit, but this does not present any fundamental difficulty in integrating eq. (4) in the x direction. The change in δ^* across the discontinuity yields the definition of a mass flux parameter Q:

$$\delta_2^* = \delta_1^* + (h - Q\delta_1^*)$$

where

$$Q = \frac{h\rho_j U_j}{\delta_j^* \rho_\infty U(x_j)} \tag{5}$$

and where the subscripts 1 and 2 refer to condition immediately upstream and downstream of the slot as shown in Fig. 1. The change in Θ across the discontinuity yields a momentum flux excess parameter M:

$$\Theta_1 = \Theta_1 - M\Theta_2$$

where

$$M = \frac{h}{\Theta_1}\left[\frac{\rho_j U_j}{\rho_\infty U(x_j)}\left(\frac{U_j}{U(x_j)} - 1\right) + \frac{P_j - p_\infty(x_j)}{\rho_\infty U^2(x_j)}\right] \tag{6}$$

Since the flow upstream of the slot will have the usual properties of a boundary layer, the Θ_1 in the definition of M reduces simply to Θ_1. The retention of the pressure term in the definition allows for the possibility of sonic or supersonic jet flows where the exit pressure might not match the local static pressure.

A kinetic energy flux parameter can be defined in much the same way. Multiplying the original momentum equation (4) by u and integrating in the y direction yields an integral "mechanical energy" equation:

$$\frac{1}{2}\frac{d}{dx}\left(\rho_\infty U^3 \delta^{**}\right) - \int_0^\delta (\rho-\rho_\infty)\frac{d}{dx}\left(\frac{U^2}{2}\right) dy + \int_0^\delta \frac{\partial u}{\partial x}(p-p_\infty)\, dy =$$

$$= \int_0^\delta u\left(\frac{\partial \tau_{xy}}{\partial y} + \frac{\partial \tau_{xx}}{\partial x}\right) dy \qquad (7)$$

where

$$\delta^{**} = \int_0^\delta \left[\frac{\rho}{\rho_\infty}\frac{u}{U}\left(1 - \frac{u^2}{U^2}\right) - 2\frac{u}{U}\frac{(p-p_\infty)}{\rho_\infty U^2}\right] dy$$

Given the usual boundary layer approximations, (7) reduces to the well known boundary layer mechanical energy integral equation. δ^{**}, like δ^* and Θ is discontinuous at the location of the slot. The change in δ^{**} across the discontinuity yields the definition of an energy parameter:

$$\delta_2^{**} = \delta_1^{**} + E\delta_1^{**}$$

where

$$E = \frac{h}{\delta_1^{**}}\left[\frac{\rho_j}{\rho_\infty}\frac{U_j}{U(x_j)}\left(\frac{U_j^2}{U(x_j)^2} - 1\right) + 2\frac{U_j}{U(x_j)}\frac{(p_j - p_\infty(x_j))}{\rho_\infty U^2(x_j)}\right] \qquad (8)$$

For the purpose of correlating the performance of jets in preventing separation, the relative momentum flux of the jet is the important physical quantity, and thus M is the pertinant dimensionless parameter.

However, the parameter M, with its dependence on the local quantities Θ, U, and p_∞, confuses the issue by being dependent on the slot location x_j. The effectiveness of a jet in delaying separation depends primarily on the jet momentum flux and less strongly on the slot location. A more useful momentum flux parameter, then, would depend only on the relative jet momentum flux, and would thus be related to the performance of the jet as a system, independent of its specific geometry. Such a system oriented parameter can be obtained by replacing the values of the local quantities in the definition of M with their values at some reference location. Since separation is the phenomenon of interest, a logical choice of reference location would seem to be the location where separation would occur in the presence of the given free-stream pressure distribution but in the absence of the jet. Quantities at this reference location will be designated by the subscript (so). It should be noted that these quantities are not necessarily those which would occur at separation if the jet were simply turned off, since, in most cases, removal of the jet would alter the location of separation sufficiently that the static pressure distribution upstream would be changed. To be precise, only in specially controllable experimental situations can the proper flow be established for the direct measurement of the (so) quantities. However, in most practical situations, quantities measured at separation with the jet removed will provide reasonably accurate approximations to these quantities. With the quantities designated by (so) as the reference, the momentum flux "system" parameter can be written:

$$M_o = \frac{h}{\Theta_{so}} \left[\frac{\rho_j U_j}{\rho_\infty U_{so}} \left(\frac{U_j}{U_{so}} - 1 \right) + \frac{p_j - p_{\infty_{so}}}{\rho_\infty U_{so}^2} \right] \qquad (9)$$

Analogous mass flow and energy "system" parameters Q_o and E_o are defined in the same way, local quantities at the slot being replaced by the (so) quantities.

The parameter M_o has proven successful in correlating the performance of two-dimensional jets in delaying separation. In Fig. 2, McGahan's [5] data has been plotted in terms of the free-stream velocity at separation U_s versus M_o. U_s has been normalized by the value of U_s which occurred with $U_j = U_{so}$ (where $M_o = 0$). (McGahan's jets were subsonic, so that the pressure term in the definition of M_o can be neglected except for U_j near zero). This choice of normalization gives the neatest correlation, since $U_j = U_{so}$ is approximately the correct amount of blowing needed to overcome the inherent drag of the slot. The correlation can be said to be quite good; data for the same slot location but different slot heights collapse nearly onto a single curve. The dependence of the effectiveness of the jet on the axial location of the slot can be seen clearly in this plot. McGahan designated the axial location of the slot by the value of the boundary layer shape factor $H = \delta^*/\Theta$ immediately upstream of the slot. The value $H = 3.05$ occurred near the point where separation occurred without blowing, and the value $H = 1.65$ occurred upstream, near the beginning of the pressure gradient. It can be seen that for higher values of M_o, slot locations near the unblown separation point should be avoided, since they do not produce as great a reduction in U_s as do the upstream slot locations.

Since U_s evaluated at $U_j = U_{so}$ is not a conveniently available quantity in most theoretical situations, a more convenient way of expressing the separation correlation is to plot U_s/U_{so}, as shown in Fig. 3. The correlation in this form is not quite as satisfying, but because of its easier application, this form of plot will be used later in the report for comparing the discrete jet data.

For the discrete jet cases all of the parameters derived in this section retain their definitions, except that the slot height h must be replaced by the nozzle area to spacing ratio A_j/S. Thus for discrete jets:

$$Q_o = \frac{A_j \rho_j U_j}{S \delta^*_{so} U_{so}} \tag{10}$$

$$M_o = \frac{A_j}{S \Theta_{so}} \left[\frac{\rho_j U_j}{\rho_\infty U_{so}} \left(\frac{U_j}{U_{so}} - 1 \right) + \frac{p_j - p_{\infty so}}{\rho_\infty U^2_{so}} \right] \tag{11}$$

$$E_o = \frac{A_j}{S \delta^{**}_{so}} \left[\frac{\rho_j U_j}{\rho_\infty U_{so}} \left(\frac{U^2_j}{U^2_{so}} - 1 \right) + 2 \frac{U_j}{U_{so}} \frac{(p_j - p_{\infty so})}{\rho_\infty U^2_{so}} \right] \tag{12}$$

EXPERIMENTAL APPARATUS AND PROCEDURE

The Tunnel

The wind tunnel used in these experiments is shown schematically in Fig. 4. The tunnel is of the open return type, with the fan at the downstream end. Except for the entrance and the diffusor, the flow channel is of constant width (30 in.), and the top wall, which includes the test wall, is flat. The flow near the flat test wall is reasonably two-dimensional, as was shown by detailed measurements taken in conjunction with a previous investigation (Ref. [7]). Two different bottom wall contours (contour 1 and contour 2 of Fig. 4) can be installed in the forward section of the tunnel, giving two different pressure distributions in that section. With contour 1, the free-stream is quickly accelerated to 191 ft/sec and remains at that velocity for a distance of about 5 ft. Rough sandpaper was glued to the top wall, covering the first 30 in. of this high speed section and serving to thicken the boundary layer. In the last 30 in. of this section the boundary layer returns to its smooth wall form, and, at the start of the test wall, the displacement thickness is 0.240 in. With contour 2, no sandpaper was used and the flow is allowed to remain at low velocity for a greater distance, resulting in a displacement thickness of 0.075 in. at the start of the test wall. This choice of boundary layer thicknesses allows some variation in the scaling of the experiments, as will be explained in the next section. The bottom wall opposite the test wall is flexible, and varying its contour gives a wide range of control over the test wall pressure distribution.

The test wall, shown in Fig. 5, consisted of an 1/8 in. thick sheet of aluminum stiffened by a supporting framework on the outside of the tunnel. The wall was perforated with a large number of 3/8 in. holes arranged in spanwise rows with close axial spacing between adjacent rows. The holes allowed a wide range of choice in the placement of jet nozzles and probe supports. Holes which were not in use during a particular run were covered with mylar electrical tape which was thin enough (.002 in.) that the wall could be considered aerodynamically smooth. The wall is shown in Fig. 5 with all of the holes covered. Static pressure taps were located at small streamwise intervals along a line one inch to one side of the tunnel centerline, and a few taps were located along lines 6 in. to either side of this main row of taps.

Since the bottom wall of the tunnel is curved, and the test wall is flat, separation would normally occur first on the bottom wall. To make possible the study of separation on the top wall, separation had to be prevented on the bottom and side walls. This was achieved by a combination of two types of wall jet blowing: Blowing through tangential slots on the bottom wall, and blowing through discrete nozzles on the side walls. There were eight bottom wall slots of the type shown in Fig. 6. These were simply open to the outside air, allowing the low static pressure in the tunnel to draw air through them. Because the main tunnel flow experienced a loss in total pressure by passing through the screens at the tunnel entrance, the air drawn through the slots emerged at a velocity somewhat higher than the local free-stream velocity. At the downstream end of the bottom wall, there was a small adjustable flap which allowed

a variable amount of outside air to join the flow into the diffuser, thereby allowing a fine adjustment of the speed of the mainstream. This flap is shown in Fig. 6. The side wall nozzles consisted of constant diameter metal tubes which were passed through the wall at an angle and then bent to lie flat against the wall, with the nozzle axes parallel to the wall. On each side wall there were two rows of 0.074 inch inside diameter nozzles (one row of six and one row of seven) and a row of four 0.125 inchinside diameter nozzles, the arrangement having been determined by trial and error through the observation of wool tufts on the tunnel walls. Because the air emerged from these nozzles at sonic velocity, the momentum added by the jets was sufficient to prevent separation, even though the mass flow added by the jets was very small compared to the mass flow in the main tunnel stream.

In the course of the experimental program, two different types of discrete jet nozzles were used on the test wall. One of these nozzle types was designed to produce as nearly as possible an "ideal" jet flow, i.e. a constant velocity core emerging from the nozzle with very thin nozzle wall boundary layers. The purpose of this nozzle type was to provide an easily interpreted "ideal" case, free from the effects of turbulence in the initial jet core or other extraneous effects. In order to achieve this type of flow, it was necessary to design the nozzle with smooth internal contours and a large contraction ratio. The resulting geometry is shown in a cross-sectional view in Fig. 7b. The 0.085 in. diameter nozzle was molded into the wall of a o.375 in. diameter stainless steel tube, with the axis of the nozzle perpendicular to the axis of the tube. The molding of the contours in epoxy plastic insured that

all of the nozzles were very nearly identical.

The second nozzle type used in the experiments was simply a constant diameter tube with a moderately sharp 90° bend (Fig. 7a), which is the simplest possible geometry for practical applications. These nozzles had an inside diameter of 0.074 in.

When nozzles of either type were mounted in the tunnel, the nozzle feed tubes projected vertically through the holes in the test wall, so that the nozzle axes were oriented in the downstream direction parallel to the wall. To prevent leakage of outside air into the tunnel, plasticene was used as a seal around the feed tubes where they passed through the holes in the wall. This arrangement allowed the tubes to slide in the holes so that the distance between the jet axes and the wall could be varied. Standard flare fittings were used to connect the jet feed tubes to a common manifold, which consisted of length of 1 in. I.D. thick walled pipe aligned transversely across the top of the tunnel. The brackets which held the manifold in place were adjustable vertically, allowing the vertical location of all of the jet axes to be set simultaneously. The manifold accommodated eleven jet tubes in a spacing pattern which matched the spacing of the holes in the test wall, as shown in Fig. 8. The spacing intervals at the ends of the row of jets were shortened because it was felt that the side walls would slow the transverse growth of the jets at the ends.

Fine adjustment of the yaw alignment of the jet axes was possible because of the rotational degree of freedom allowed by the flare fittings

which held the jet feed tubes. To accomplish this alignment, the jet manifold was mounted on a special jig, which is shown in Fig. 9 with one jet tube in place. The alignment probe shown in Fig. 9 consisted of two open ended tubes of 1/2 in. diameter mounted parallel to each other with their axes 1 in. apart. These tubes were connected across a sensitive mass flow meter, which in this case served as a sensitive null pressure indicator. The probe was placed two feet from the jet nozzle so as to straddle the desired location of the jet axis. With the jet running ($U_j \approx 900$ ft/sec) in the otherwise quiescent air of the room, the jet axis alignment was adjusted until the pressure across the alignment probe showed a null. It was found that the jet axes could be aligned to within ±1/2 degree in this way. This method was used to align each jet tube as it was installed, while all previously installed nozzles were taped closed to prevent their influencing the alignment procedure.

Air was supplied for both the test wall jets and the side wall jets from the laboratory compressors and storage tanks at a pressure ranging from 2,000 to 3,000 psi. Simple throttling valves were used to reduce this pressure for the side wall jets. For the test wall jets, a regulator was used to reduce and control the pressure in the jet manifold, which was monitored on either a 0-60 psi or a 0-150 psi Heise pressure guage depending on the range of pressures used. A variable electric heater was used to control the jet stagnation temperature, which was monitored by a thermocouple in the jet manifold.

Measurements

A large part of the experimental program involved setting up a number of flows in which the overall performance of the jets could be determined, but in which detailed flow field measurements were not made because of the large number of different flows to be investigated. In these cases, the wall static pressure was the primary measurement. In the cases with zero jet velocity (the no blowing test cases), the wall static pressure measurements were supplemented with a flow visualization technique using small paper flags, as explained in [7]. The separation point locations inferred from the static pressure distributions and the visual technique were in agreement, just as they had been in the work reported in [7]. But in cases with substantial amounts of blowing, the extra turbulence introduced by the jets rendered the flag technique unusable, and the static pressure became the sole measurement. This was not an important shortcoming, however, because of some of the changes in the nature of the flow brought about by blowing. When the blowing was substantial, separation was delayed for considerable distances downstream, and, as a result, the pressure distribution upstream of separation could not be controlled as closely as it had been in the no blowing cases.

The usual leveling off of the pressure distribution at separation tended to occur much more gradually in the cases with blowing, in spite of efforts to find a bottom wall contour which would force the free-stream velocity gradient to remain constant up to the separation point. However, the final pressure reached after the pressure had leveled off

seemed to be insensitive to the details of the upstream pressure distribution, and thus a more useful measure of the performance of the jets seemed to be the final recovery pressure rather than the exact location of separation. In this way, the measured axial distributions of static pressure provided an accurate measure of the effectiveness of the jets.

The wall static pressures, which could be monitored at the numerous static pressure taps built into the test wall structure, were measured on a vertical tube manometer board using alcohol as the working fluid. The pressure readings were found to be repeatable to within about 0.02 inches, or 0.2% of the maximum free-stream dynamic head.

All flow field mean velocity measurements were made with small pitot tubes. For purposes of checking and calibrating the performance of the jet nozzles, a number of single free jet velocity profiles were measured in quiescent air. For these cases, a single pitot tube and a single static pressure tube were traversed separately, and their records were combined to obtain velocity profiles. The pitot tube was round, with an outside diameter of 0.020 in. and an inside diameter of 0.010 in., the tube tip having been ground flat perpendicular to the tube axis. The static pressure tube was 0.032 in. in diameter with a rounded tip and with four 0.013 in. diameter holes drilled 0.25 in. back from the tip. For the velocity profiles measured in the tunnel with a co-flowing stream, the wall static pressure taps were adequate for measuring the static pressure, and the static pressure tube was not used.

In order to measure the spanwise variations in the co-flowing case, an array of five pitot tubes (of the same design as in the quiescent air

cases) was used. The tubes were mounted on a single probe holder so that they could be traversed vertically in unison. A photograph of this array is shown in Fig. 10. The pitot tubes were equally spaced in the spanwise direction so as to cover a spanwise band 1.5 in. wide, thus covering the spanwise region between one nozzle axis and a point half the distance to an adjacent nozzle axis (see Fig. 8). In practice, the pitot tubes were monitored separately, and five traverses were required to measure profiles at the five spanwise stations. The probe array allowed this to be done without having to stop the tunnel between traverses.

The probe traverse mechanism, which was used for both the quiescent air cases and the co-flowing cases, consisted of a modified compound lathe rest with an electric motor drive. The vertical position of the probe holder was measured by a Sanborn 7DC DT 2000 linear transformer, which was calibrated during each traverse against the feed screw of the traversing mechanism. Fig. 9 shows the traverse mechanism and linear transformer in position on the jet alignment jig for the quiescent air cases. The traverse mechanism and the jet manifold are shown in position on the wind tunnel in Fig. 11. The output of the linear transformer was connected to drive the x axis of an x-y plotter. The y axis of the plotter was driven, through a DC amplifier, by a pressure transducer which was connected to the probe being monitored. The pressure transducer was either a Statham 2732 P6-1.5 D-120 or a Pace CP51D - .1 PSI depending on the range of pressure to be measured on that particular traverse. The transducer in use was calibrated at the end of each traverse against a Merriam 34FB2 micromanometer.

In order to be able to make the comparisons drawn in the next section, it was necessary to know the jet mass, momentum, and energy fluxes at different jet stagnation pressures. In the case of the flared jet nozzle with the large contraction ratio, it is reasonable to assume one-dimensional isentropic flow to calculate the nozzle exit conditions from the stagnation conditions. The integrated impulse from the measured velocity and static pressure profiles measured in quiescent air at stations 4.40 and 8.80 in. from the nozzle exit agreed very closely with these one-dimensional calculations. Values calculated in this way were therefore used for all of the flared nozzle comparisons.

In the case of the bent tube nozzles, friction was an important factor. It seemed reasonable in this case to assume one-dimensional adiabatic friction flow (see Shapiro [8]) to calculate the nozzle exit conditions, using the results of the quiescent air profile measurements to "calibrate" the calculations. Profiles measured 4.40 in. from the nozzle exit at one particular value of jet stagnation pressure were used to calculate the pressure and density at the nozzle exit, where the flow was assumed to be sonic. Given these nozzle exit conditions and the known initial stagnation conditions, the effective friction factor for the jet tube was determined from tables [8] of one-dimensional friction flow. For purposes of calculating the nozzle exit conditions at other stagnation pressures, this friction factor was assumed to vary as the inverse fifth power of the tube Reynolds number (an empirical approximation for turbulent flow given in [7]). Since the velocity and temperature at any point in the tube changed very little over the

whole range of stagnation pressures, the tube Reynolds number was taken to be proportional to the stagnation pressure. Using these assumptions concerning the friction factor, nozzle exit conditions were determined from the one dimensional flow tables for the several values of stagnation pressure which were used in the course of the experiments.

Running Procedures

In the cases where only the overall performance of the jets was to be determined, the only flow quantities which had to be measured were the jet stagnation pressure and the distribution of static pressure (with reference to the free-stream pitot pressure) on the test wall. For a typical run, the jet nozzles were installed at the desired axial location, and all other holes in the test wall were taped closed. The jet air flow and the air supply heater were then turned on, the stagnation pressure was set via the regulator, and the system was allowed to run until the jet stagnation temperature settled to room temperature. This usually required some trial and error adjustment of the heater, depending on the pressure in the storage tanks. With the jet flow established, the side wall jets and the main tunnel flow were turned on, and the tunnel speed was set by the adjustment of the flap at the entrance to the diffuser. The bottom wall contour was then adjusted to give the desired pressure distribution upstream of separation. When the desired distribution was established, the static pressures were recorded from the manometer board. The vertical location of the jet nozzles could be changed while the tunnel was running, and data for three different locations were generally recorded in the course of a single run.

In the one case where extensive flow field measurements were made, the pitot tube array described earlier was installed at a different axial location at the beginning of each run. The basic procedure for these runs was the same as for those described above, except that running times had to be considerably longer to allow the required five pitot tube traverses to be made at each station.

THE EXPERIMENTAL PROGRAM

As was stated in the introduction, the first phase of the experimental program was exploratory, in which only the overall performance of the jets was measured while the important parameters were varied in a systematic way. The important geometric variables to be covered were the axial location of the nozzles x_j, the vertical distance y_j between the nozzle axes and the wall, and the spanwise nozzle spacing S. On the basis of the two-dimensional results (MaGahan [5]) discussed in the Analytical Background section, it appeared that the combined effects of the nozzle diameter d and the nozzle exit velocity U_j and density ρ_j could be characterized sufficiently by the momentum flux parameter M_o. It was therefore decided not to attempt to vary d, U_j, or ρ_j independently of M_o. The important variables to be covered in the exploratory phase of the program were thus x_j, y_j, S, and M_o.

The variation of x_j and y_j was accomplished directly by placing the jet nozzles in a wide range of different locations. At each location, a tunnel run was performed according to the procedure described in the previous section. At some locations, several different jet stagnation pressures were used, so that a range of M_o was covered.

For reasons of mechanical simplicity, it was decided not to try to vary S directly. Instead, the two alternate bottom wall contours (contours 1 and 2 of Fig. 4) were used to establish flows with widely different boundary layer thicknesses. With contour 1, the displacement thickness at the beginning of the pressure gradient was 0.240 in., and with contour 2 the displacement thickness was 0.075 in. These two flows will

be referred to hereafter as the "small nozzle spacing" case and the "large nozzle spacing" case respectively, the displacement thicknesses at the beginning of the pressure gradient differing by a factor of 3.20.

The streamwise distribution of static pressure upstream of separation which was used in the small nozzle spacing case was the same as that used in the large nozzle spacing case, except that the streamwise scale of the distribution was stretched by a factor of 3.20, making the two flows geometrically similar with regard to the initial displacement thickness and the streamwise scale of the pressure distribution. Without jets, these two flows were expected to remain similar to each other up to separation, except for small differences caused by the difference in Reynolds number. The profile measurements made without the jets showed this to be the case. When the jets were installed, the flows were purposely not geometrically similar because the 3.0 in. spanwise spacing of the nozzles remained the same in both cases. The nozzle spacing appeared effectively smaller by a factor of 3.20 in the small nozzle spacing case than it did in the large nozzle spacing.

The streamwise static pressure distributions used in both cases, translated into free-stream velocities via the Bernouli equation, are shown in Figs. 12 and 13, along with the resulting boundary layer displacement and momentum thicknesses. After a brief transition from the constant pressure section, the free-stream velocity was made to follow a linear distribution as nearly as possible until separation occurred. The slope of this distribution was scaled by the factor 3.20 between the two cases, and the final free-stream velocity reached after separation was nearly the same in both cases. The separation locations, x_{so}, shown

in Figs. 12 and 13 were determined by the flag technique. Hereafter, the subscript (s0) will refer to quantities at these locations (e.g. Θ_{so}), except for U_{so}, which will refer to the minimum U reached after separation as shown in Figs. 12 and 13. The momentum thickness and the boundary layer shape factor H from the beginning of the pressure gradient to the separation point are plotted nondimensionally in Fig. 14, showing the reasonably close geometric similarity between the two cases. Here, the effective beginning of the pressure gradient was taken to be x_o, the origin of the attempted linear velocity distribution, and Θ_o is the value of Θ at x_o. Parameters of the initial unblown boundary layers are summarized in the following table:

Table I: Unblown Boundary Layer Parameters

Case	x_o	x_{so}	δ^*_{so}	Θ_{so}	$\frac{x_{so}-x_o}{\delta^*_{so}}$	$\frac{x_{so}-x_o}{S}$
Large Nozzle Spacing	1.5"	8.7"	.415"	.156"	17.3	2.40
Small Nozzle Spacing	5.0"	29.0"	1.27"	.600"	17.3	7.43

In the cases with blowing, the bottom wall was adjusted at the beginning of each run to make the free-stream velocity follow the prescribed linear distribution as far downstream as possible. In some cases with large jet momentum fluxes, the static pressure remained somewhat higher than the prescribed distribution for some distance downstream of the nozzles. This effect was presumably due to streamline curvature caused by the strong jet entrainment and could not be adjusted out without upsetting the pressure distribution upstream. In addition, as was mentioned earlier, the cases where separation was delayed for a considerable distance displayed a more gradual levelling off of the pressure than the more moderately delayed cases. However, these uncertainties in the pressure distribution upstream of separation were not considered important because some special runs, in which the pressure distribution was allowed to vary, showed that the final pressure recovery achieved after separation was not sensitive to the details of the upstream distribution.

The parameter space covered in the course of the exploratory portion of the program is outlined in the following Table, where the axial location of the jet nozzles is expressed in terms of the distance between the nozzles and the station where separation occurred without the jets, normalized by the nozzle spacing:

Table II: Nozzle Combinations Tested

Boundary layer case	Relative spanwise spacing	Nozzle type	$\frac{x_j - x_{so}}{S}$	$\frac{y_j}{S}$	M_o
thin	large	flared	-2 to 1	.0141 to .141	0.551 to 1.74
thick	small	flared	-8.5 to 0	.0141 to .283	0.79
thick	small	bent tube	-8.5 to 0	.085 to .482	0.138 to 0.954

Negative values of $(x_j - x_{so})/S$ correspond to nozzle locations upstream of the unblown separation point. The nozzle locations ranged from near the beginning of the pressure gradient to somewhat downstream of the unblown separation point. The nozzle axis heights covered a range from the minimum that was mechanically practical to a sufficient distance from the wall that the performance was noticeably below the optimum. For the flared nozzles, the minimum axis height corresponded to having one edge of the nozzle exit flush with the wall surface $(y_j/S = 0.0141)$. The bent tube nozzles could not be placed flush with the wall because of the bend in the tube, and thus the minimum height had to be somewhat greater $(y_j/S \approx 0.085)$.

Low values of M_o in the large nozzle spacing case (thin boundary layer) resulted in unsteady running of the tunnel. Flow visualization, using the flag technique, showed that separation was occurring between the jets before the jets had had sufficient distance to merge, and reattachment downstream was only intermittent. For this reason, no reliable runs could be made in this case for values of M_o below 0.5.

In the small nozzle spacing cases, a basic limitation of the tunnel placed an upper limit on the values of M_o which could be tested. Because of the thicker tunnel wall boundary layers in this case, the maximum pressure recovery which could be achieved in the tunnel was not as large as in the large nozzle spacing case. There was a limiting value of pressure recovery above which the flow filled the entire channel without separating. In this case, runs were not made for values of M_o above 0.954 because separation did not occur at higher values.

On the basis of the results of the exploratory phase of the program, one of the large nozzle spacing cases with $M_o = 1.74$ was chosen for an extensive set of mean velocity profiles. The particular case characterized by $(x_j - x_{so})/S = -2$ and $y_j/S = 0.085$ was chosen because it achieved the highest pressure recovery of any of the flows investigated in the program. A set of five profiles was measured at each of six axial stations.

Some general features common to all of the flows investigated can be seen in Fig. 15, which is an isometric view of the measured mean velocity profiles for the case which achieved the highest pressure recovery. Profiles for the corresponding unblown case are included for comparison. In the profiles with blowing, the jets are seen to merge, eventually producing a nearly two-dimensional flow, and separation is delayed until far downstream. The free-stream velocity distribution for this case, as deduced from wall static pressure measurements, is shown in Fig. 16a. The final pressure recovery amounts to over 95% of the initial (maximum) free-stream dynamic pressure. Since the flag technique did not prove useful in locating separation with blowing, U_s in the comparisons that follow was taken to be the final, maximum value of U. The other combinations of nozzle location and momentum flux resulted in free-stream velocity distributions analogous to that shown in Fig. 16a, but with lower final pressure recoveries. The free-stream velocity measurements for the other cases are shown in Figs. 16b through 16u.

Effect of Nozzle Location

The effect of nozzle location on the performance of the jets is shown in Figs. 17 and 18, where the final free-stream velocity achieved downstream (calculated from static pressure data and normalized by its unblown value) is plotted versus nozzle axial location for the flared nozzles and the bent tube nozzles respectively. The axial locations of the nozzles are plotted in terms of the distance between the nozzles and the unblown separation point, normalized by the spanwise nozzle scaling of 3 in., and a separate performance curve is shown for each value of the nozzle axis height y_j.

Figures 17 and 18 show that over a wide range of axial locations upstream of the unblown separation point the performance of the jets was not strongly sensitive to axial location. Over this upstream range of locations performance generally continued to improve as the nozzles were moved upstream, but the rate of improvement was not large. As the nozzles were moved downstream into the immediate vicinity of the unblown separation point, performance deteriorated noticeably. This effect was strongest in the large nozzle spacing case, which corresponds to the thin boundary layer. It appears that in this case the jets did not have sufficient distance in which to merge when the nozzles were placed less than about two nozzle spacings upstream from the unblown separation point.

It is difficult to make a direct comparison between the dependence on axial location found in the present study of discrete jets and that found by McGahan for two-dimensional jets. Even minor differences in the form of the free-stream velocity distribution could produce effects which would cloud the comparison if it were made directly in terms of a nondimensionalized axial distance scale. It would seem more reasonable to devise a dimensionless scale in terms of the value of the free-stream velocity at the nozzle location and its values at the beginning of the pressure gradient and at the unblown separation point. This is done in Fig. 19, where the final free-stream velocity, normalized as in Fig. 2, is plotted against the quantity $(U_o - U_j)/(U_o - U_{so})$, which is equal to zero at the beginning of the pressure gradient and equal to one at the unblown separation point. The data plotted for discrete jets are for

the flared nozzles at the vertical location which gave the best performance, and the data for two-dimensional jets were cross-plotted from McGahan's data in Fig. 2.

Both types of jet display a reduction in performance if placed too close to the unblown separation point. At $M_o = 0.79$, the performance of the two-dimensional jet also begins to fall off as the slot is moved upstream of the optimum location, while the discrete jet performance displays no such fall-off. This would indicate that skin friction imposes more of a penalty on the two-dimensional jet than it does on advantageously placed discrete jets. This trend does not appear at $M_o = 1.74$, possibly because the two-dimensional data do not go as far upstream as they did for $M_o = 0.79$.

The effect of the vertical location of the nozzles is also shown clearly in Figs. 17 and 18. The best location tested corresponded to $y_j/S = 0.085$, where the nozzle axes were 0.25 in. from the wall. Performance was noticeably lower with one edge of the nozzle opening flush with the wall, probably due to greater skin friction losses in this case. Performance also deteriorated when the nozzles were moved farther from the wall. This fall-off in performance is due at least partially to the fact that as the nozzle axis height is increased, a greater length of each jet feed tube is exposed to the tunnel flow, increasing the parasite drag of the nozzle installation. This explanation is supported by the observation that the decrease in performance with increasing nozzle axis height was more rapid in the case of the flared nozzles, with their larger diameter feed tubes, than it was with the bent tube nozzles.

Another contributing factor in the decrease of performance with increasing height is probably the geometry of the jet flow itself. Results with discrete jets in still air [1] have shown that the interaction of the jet with the wall increases the jet's lateral growth rate. When the height of the jet axis above the wall is increased, this interaction is postponed until farther downstream, and the effective merging of adjacent jets could also be expected to move downstream, rendering the jets less effective in preventing separation.

Effect of Momentum Flux

It was shown in the Analytical Background section that the natural way to correlate the effect of jet momentum flux is by means of the momentum "excess" parameter M_o, (eqs. 9 & 11) which arises naturally for the equations of motion. In Fig. 20, the performance of discrete jets at their most advantageous location (axially farthest upstream with y_j = 0.25") is compared with the performance of McGahan's [5] two-dimensional jet at its most advantageous slot location (H = 1.90). The performance of the discrete jets is slightly better in the middle range of M_o, probably because of smaller skin friction losses. The one discrete jet data point for M_o greater than one is for the case with relatively wide nozzle spacing (thin boundary layer case) and is therefore probably not representative of the best that could be done with discrete jets in the high M_o range.

The discrete jets, because of their higher nozzle exit velocity ratio U_j/U, provided a greater energy flux than did the two-dimensional jet at a given value of M_o. Some of this extra energy undoubtedly became

turbulence kinetic energy, thus enhancing the mixing process. It seems unlikely, however, that this extra energy was the decisive factor in giving the discrete jets an advantage over the two-dimensional jet. In McGahan's [5] experiments the wider jet slot, with its lower velocity and thus lower energy for a given M_o, gave slightly better performance than the narrower slot. Thus it seems reasonable that more vigorous mixing is only helpful in some cases where separation occurs because of the jets' inability to mix fast enough with the surrounding flow. McGahan's examples of downstream placement of the slot, resulting in separation occurring between the jet and the outside flow rather than at the wall, and the discrete jet flows in which separation seemed to be taking place between the jets are examples of flows in which increasing the energy input for a given M_o might be helpful. But the situation is different in the more advantageous upstream jet locations. In these cases there is room for sufficient mixing to take place before separation occurs, and if the energy is increased without increasing M_o, the jet diffuses sooner and is acted upon more strongly by the pressure gradient downstream.

The higher energy input of the discrete jets is shown in Fig. 21 in terms of the system oriented energy parameter E_o. Since performance was correlated reasonably closely by the parameter M_o, it is to be expected that the higher U_j/U of the discrete jets resulted in a larger value of E_o for a given level of performance. On the other hand, the larger U_j/U used with the discrete jets resulted in much lower mass flow

rates for a given level of performance than were required in McGahan's two-dimensional experiments. This effect is illustrated in Fig. 22, which shows performance of the jets in terms of the system oriented mass flux parameter Q_o.

CONCLUSIONS

In terms of delaying separation in an adverse pressure gradient, it has been found that an advantageously placed installation of discrete nozzles will perform as well as or slightly better than a comparable two-dimensional slot installation for the same value of the momentum "excess" parameter M_o. The high nozzle exit velocities which are practical with discrete nozzles provide good performance at lower mass flow rates than are required at lower velocities, but some penalty is paid for this in terms of higher jet energy flux and the resulting higher power required.

The design of a discrete jet installation should present no special problems provided the following guidelines are kept in mind:

1. The combination of nozzle axial location and spanwise spacing should be chosen such that the nozzles are at least two spanwise spacings upstream of the location where separation would occur without the jets.
2. The nozzles should be placed near the wall, but not so near as to cause large skin friction losses. A nozzle axis height above the wall of about 0.1 of the spanwise spacing is a good choice, provided that this amounts to at least two or three nozzle diameters.
3. The exterior of the nozzles should be designed for low drag, provided that this can be done without causing large losses in the internal flow.

The effect of streamwise wall curvature was not investigated in this report. Convex curvature, if it were present, would have to be considered carefully in the design of a discrete jet installation.

If the curvature were mild, the flow would not be expected to differ appreciably from the corresponding flow over a flat wall. But if the radius of curvature were not large compared to the nozzle spacing, the situation could be quite different. The Coanda effect, in which a two-dimensional jet tends to remain attached to a curved wall, would not be operative with discrete jets until adjacent jets merged to some extent. It would seem advisable, therefore, either to make the nozzle spacing small compared to the radius of curvature, or, if this is not practical, to install the nozzles upstream so that the jets have sufficient distance in which to merge before encountering the region of sharp curvature. Experimentation will be needed to outline accurately the effect of curvature on discrete jet flows.

REFERENCES

[1] McLean, J. D. and Herring, H. J., "Discrete Wall Jets in Quiescent Air", NASA CR-2388, (1974).

[2] Lachman, G. V., ed., Boundary Layer and Flow Control, Pergamon Press, London, (1961).

[3] Abramovich, G. N., The Theory of Turbulent Jets, M.I.T. Press, (1963).

[4] Newman, B. G., "The Prediction of Turbulent Jets and Wall Jets", Canadian Aeronautics and Space Journal, Vol. 15, No. 8, (1969).

[5] McGahan, W. A., "The Incompressible, Turbulent Wall Jet in an Adverse Pressure Gradient", M.I.T. Gas Turbine Laboratory, Report No. 82, (1965).

[6] Schlichting, H., Boundary Layer Theory, McGraw-Hill Book Co., Inc., New York, (1960).

[7] McLean, J. D., "The Transpired Turbulent Boundary Layer in an Adverse Pressure Gradient", Ph.D. Thesis, Department of Aerospace and Mechanical Sciences, Princeton University, Princeton, N.J., (1970).

[8] Shapiro, A. H., The Dynamics and Thermodynamics of Compressible Fluid Flow, The Ronald Press Co., New York, (1953).

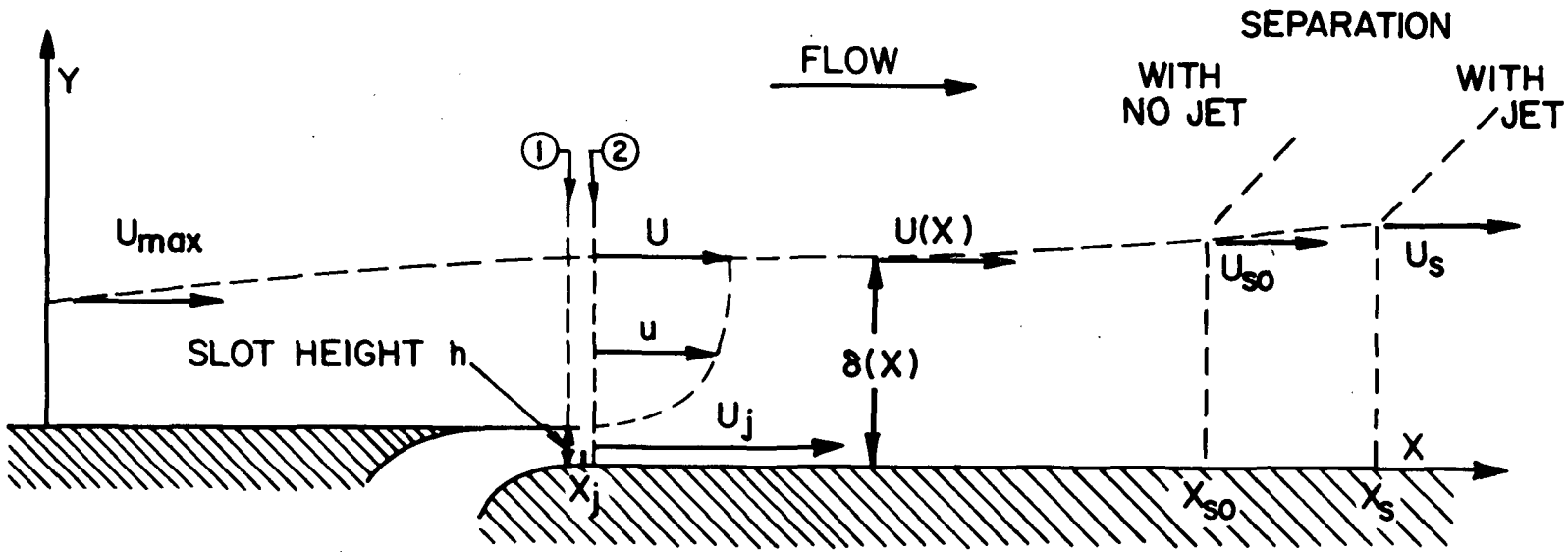

Figure 1. Schematic of a two-dimensional wall jet flow, illustrating terminology used in the derivation of dimensionless flow parameters

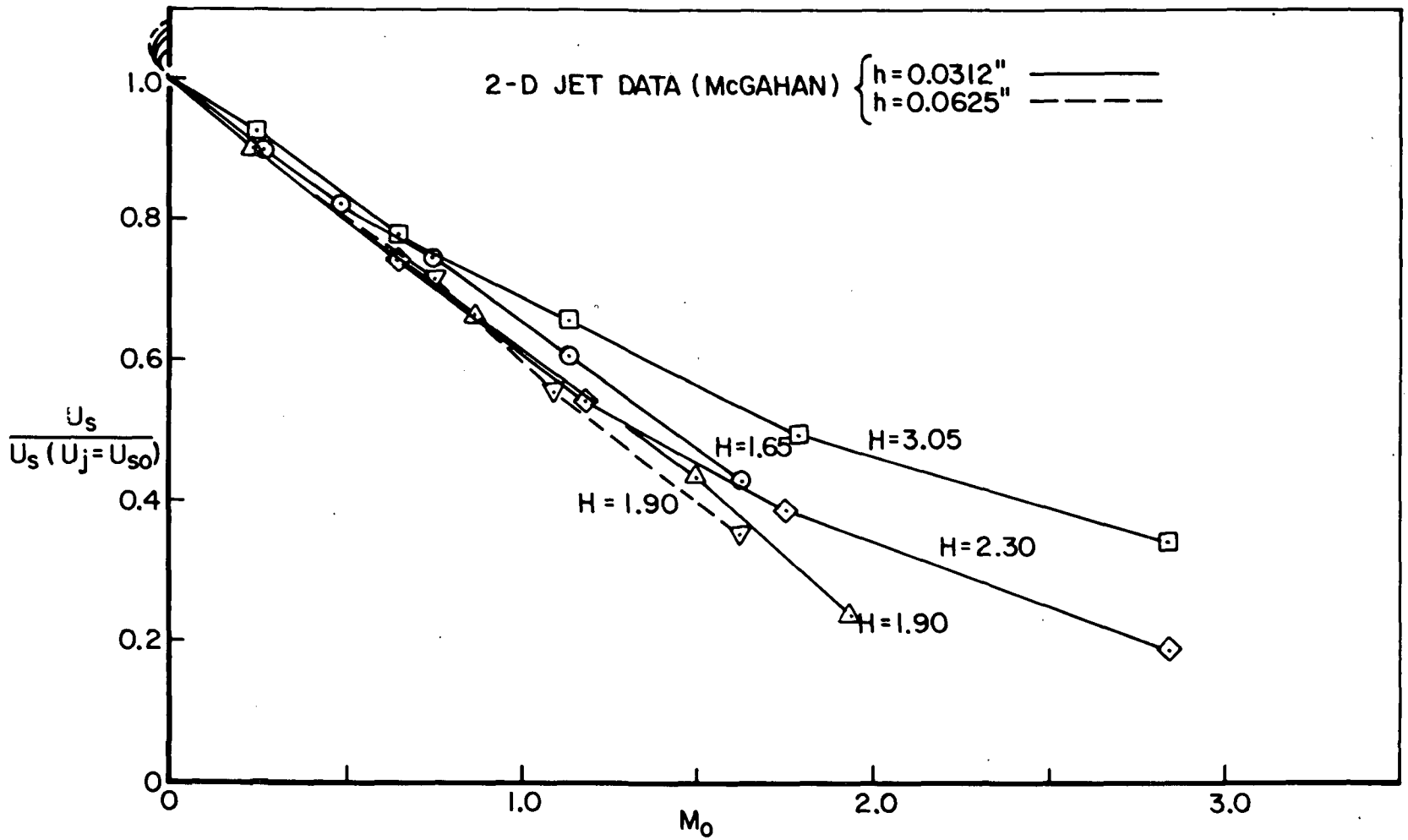

Figure 2. Correlation of two-dimensional jet performance with the parameter M_o. The free-stream velocity achieved at separation is normalized by that which was achieved with $U_j = U_{so}$.

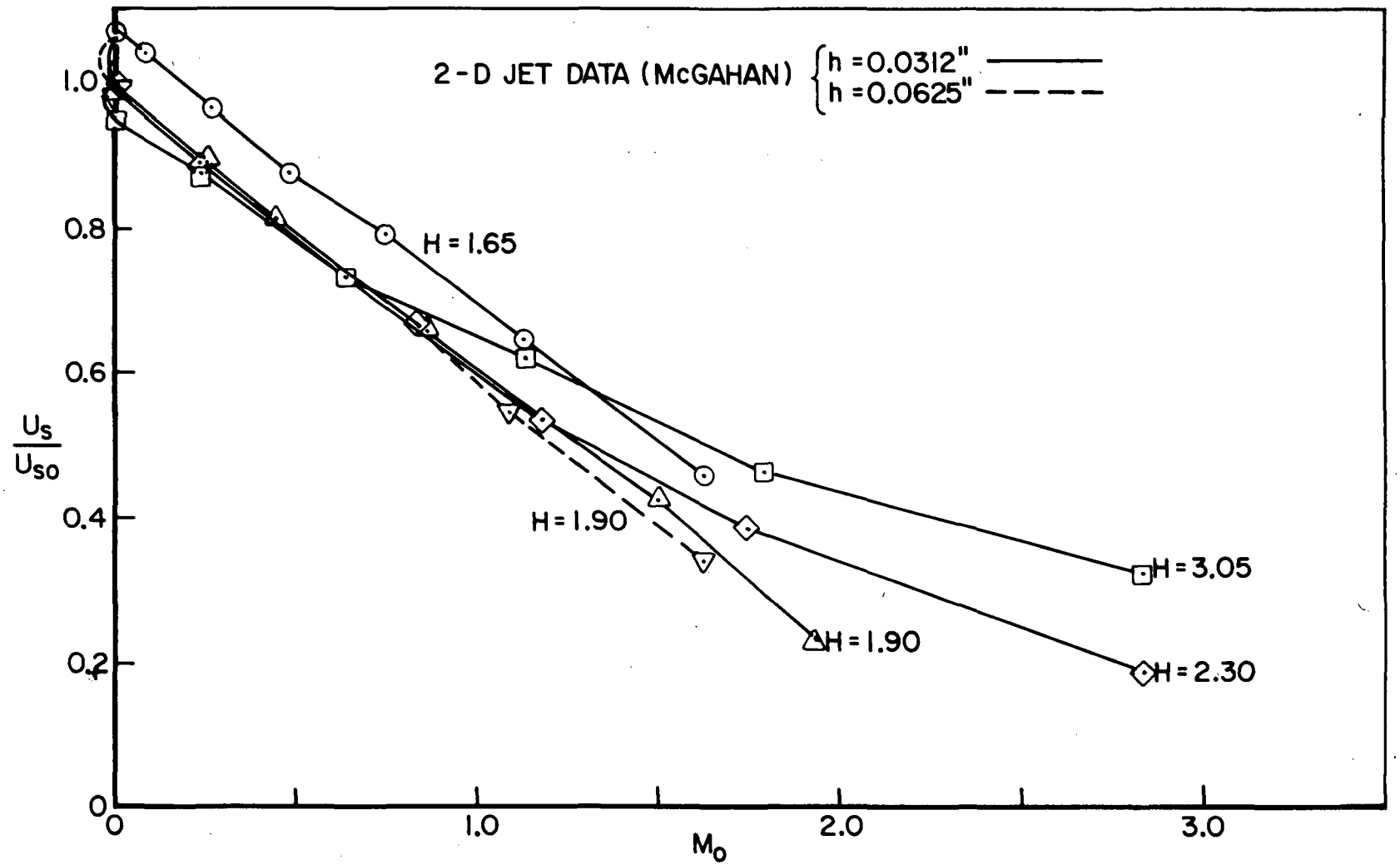

Figure 3. Correlation of two-dimensional jet performance with the parameter M_o, with U_s normalized by its value at $U_j = 0$.

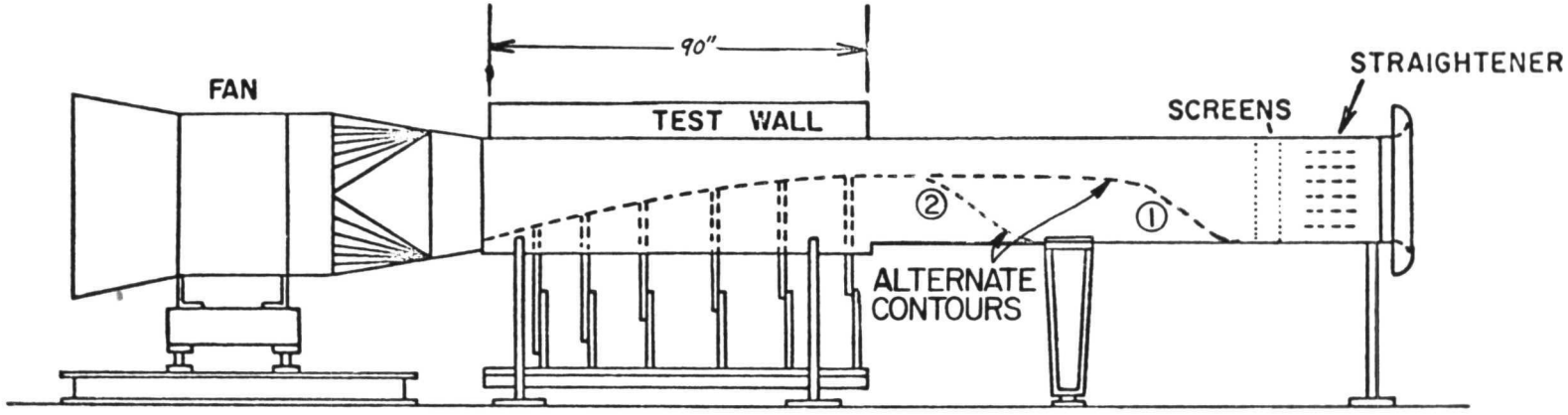

Figure 4. Schematic of the wind tunnel used in the discrete jet experiments.

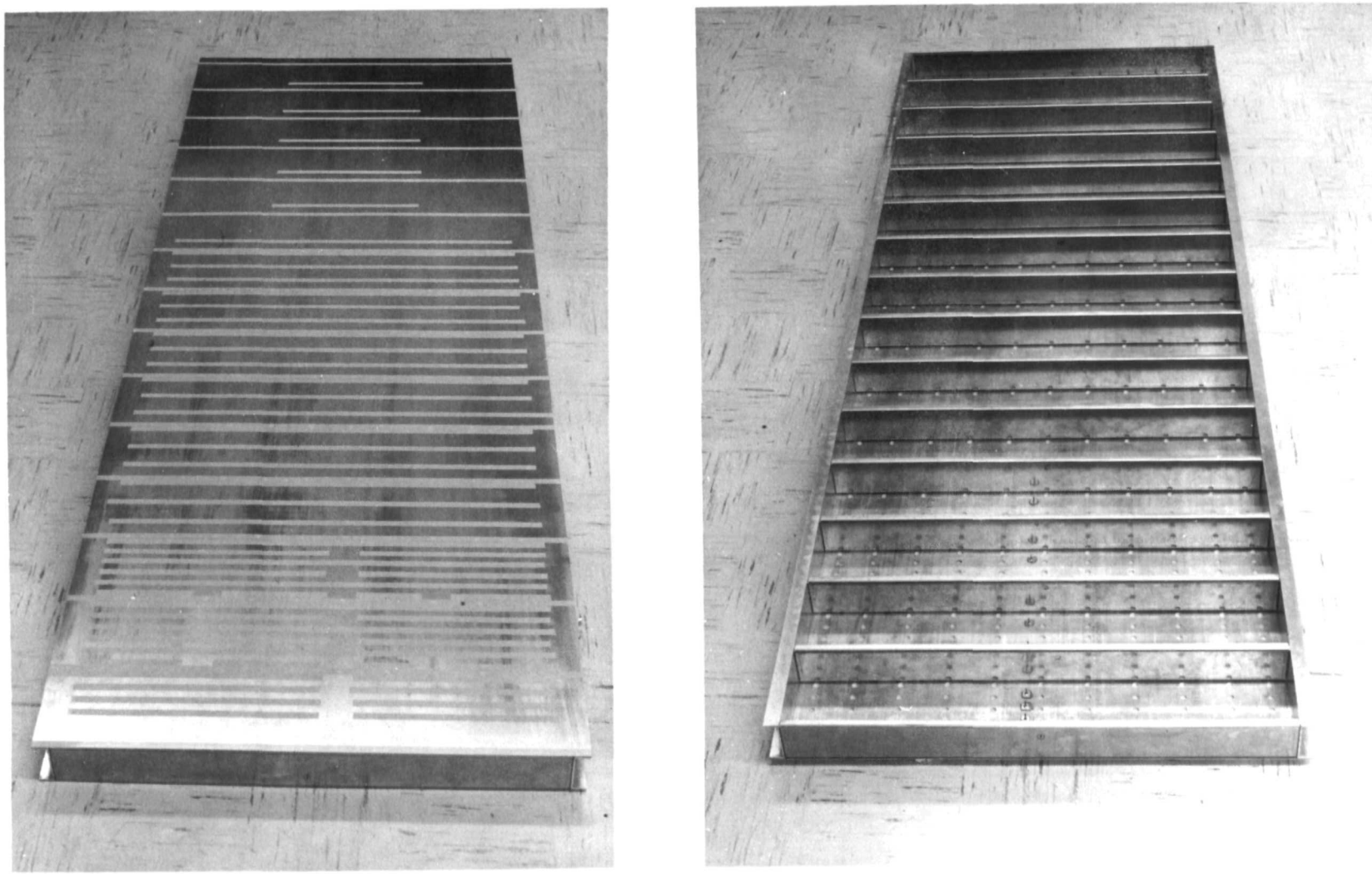

Figure 5. Photos of the test wall structure. On the left is shown the flow side with plastic tape covering the access holes for jet nozzles and pitot probes. On the right is shown the supporting structure.

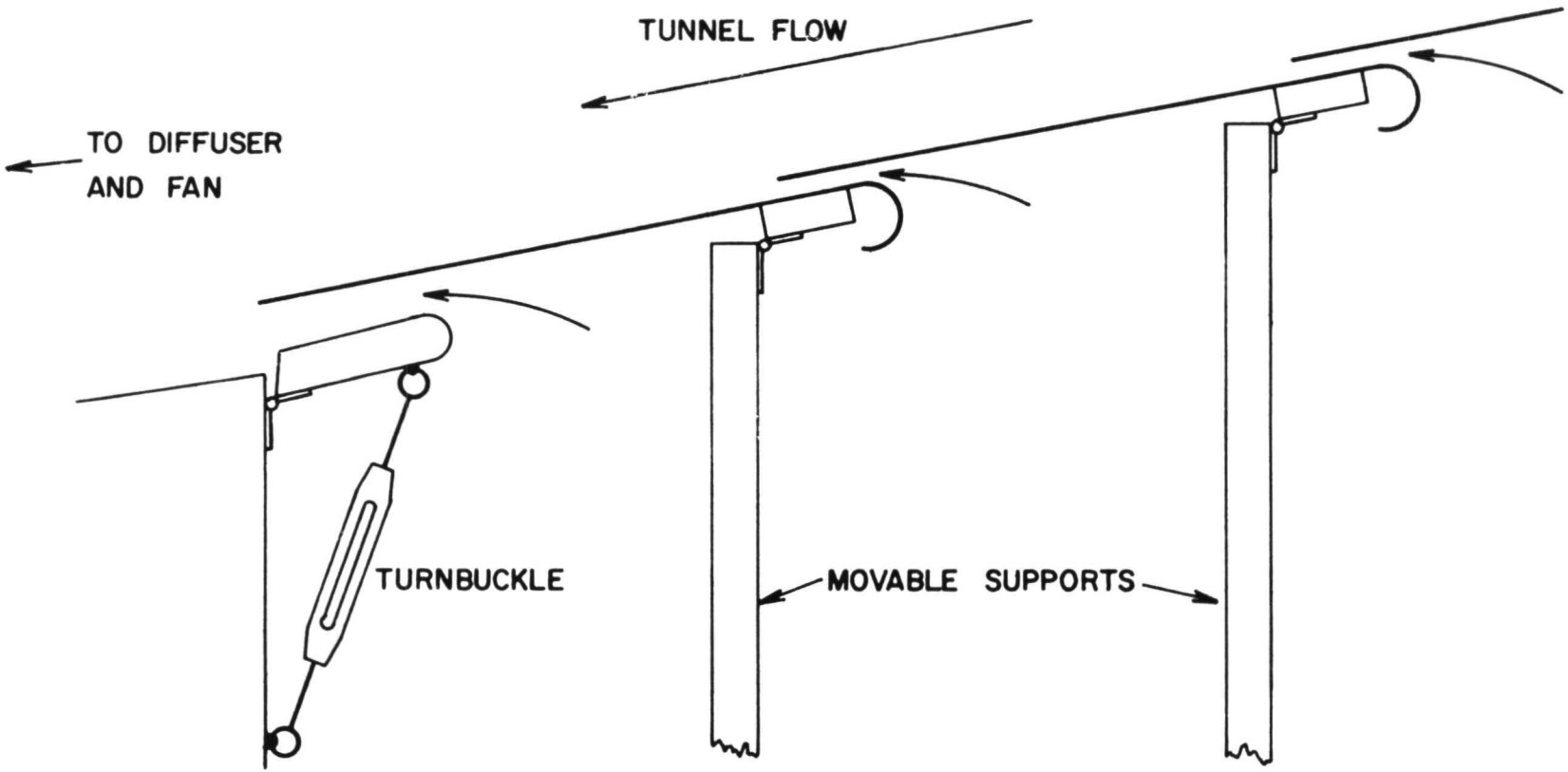

Figure 6. Schematic of the bottom wall, showing the flap used for fine control of the tunnel speed and two of the eight slots for prevention of separation.

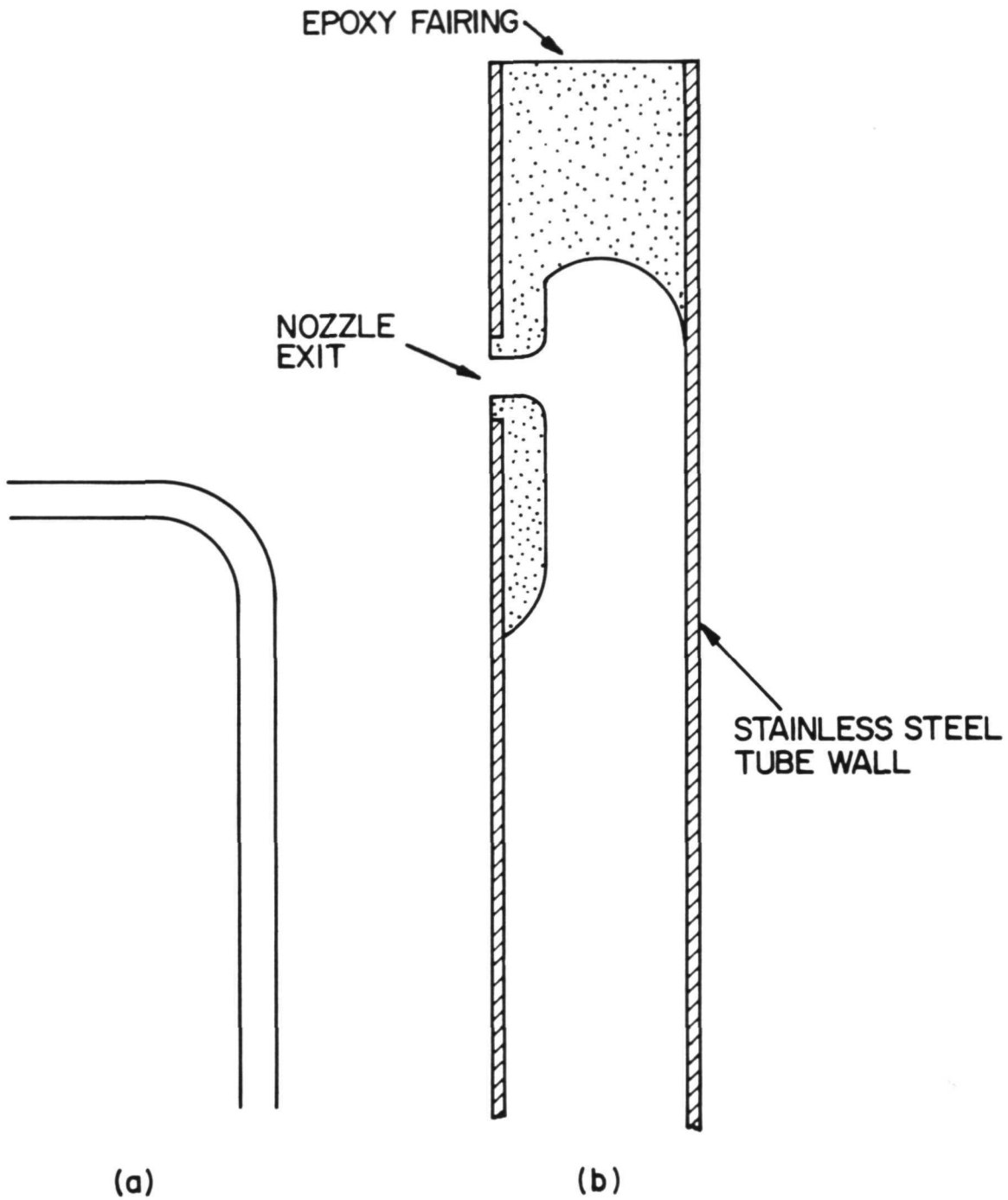

Figure 7. Cross-sections of the two types of jet nozzles used:
(a) Bent tube nozzles: 0.074" inside diameter.
(b) Internally flared nozzles: 0.085" nozzle exit diameter.

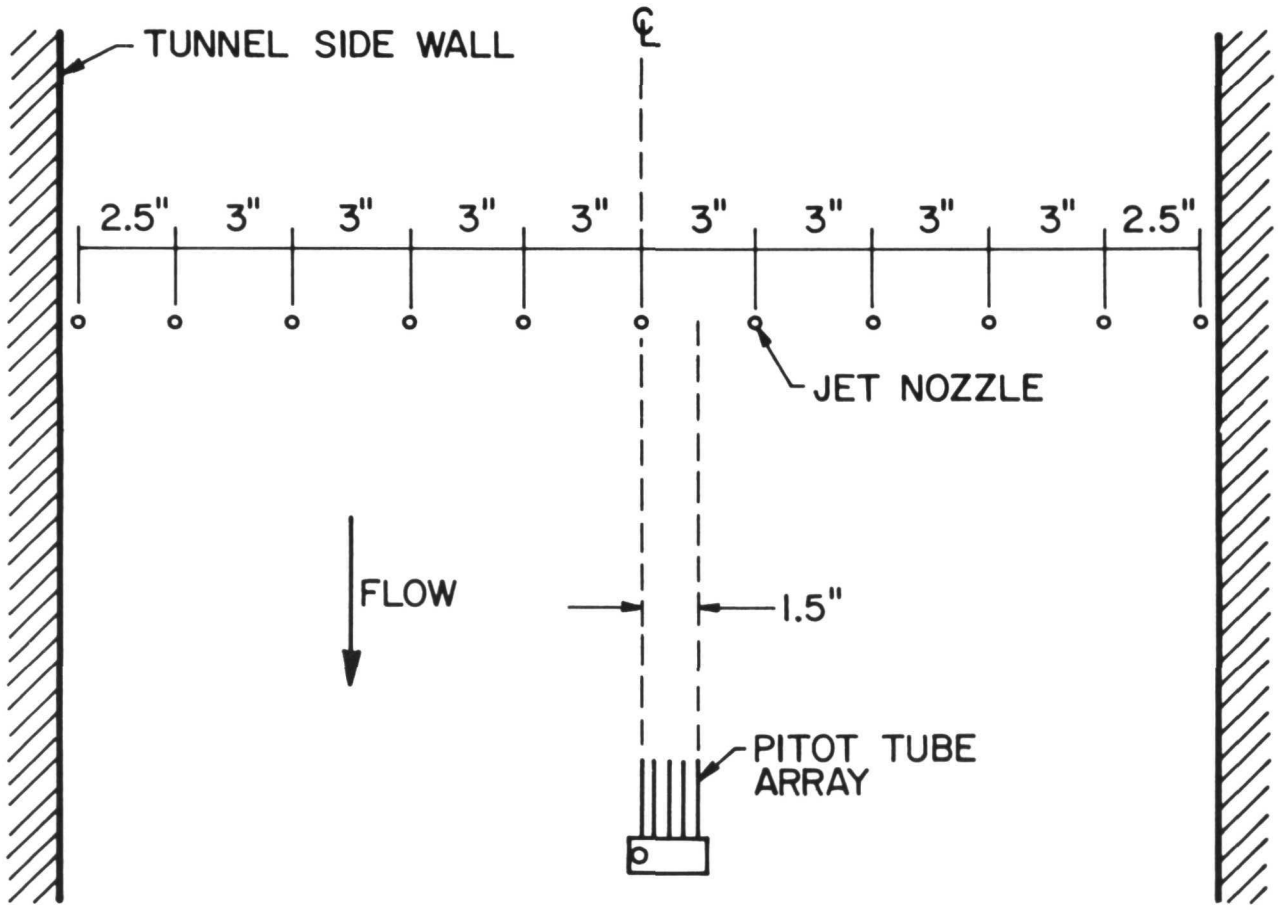

Figure 8. Diagram (looking vertically) of the arrangement of jet nozzles and pitot tubes.

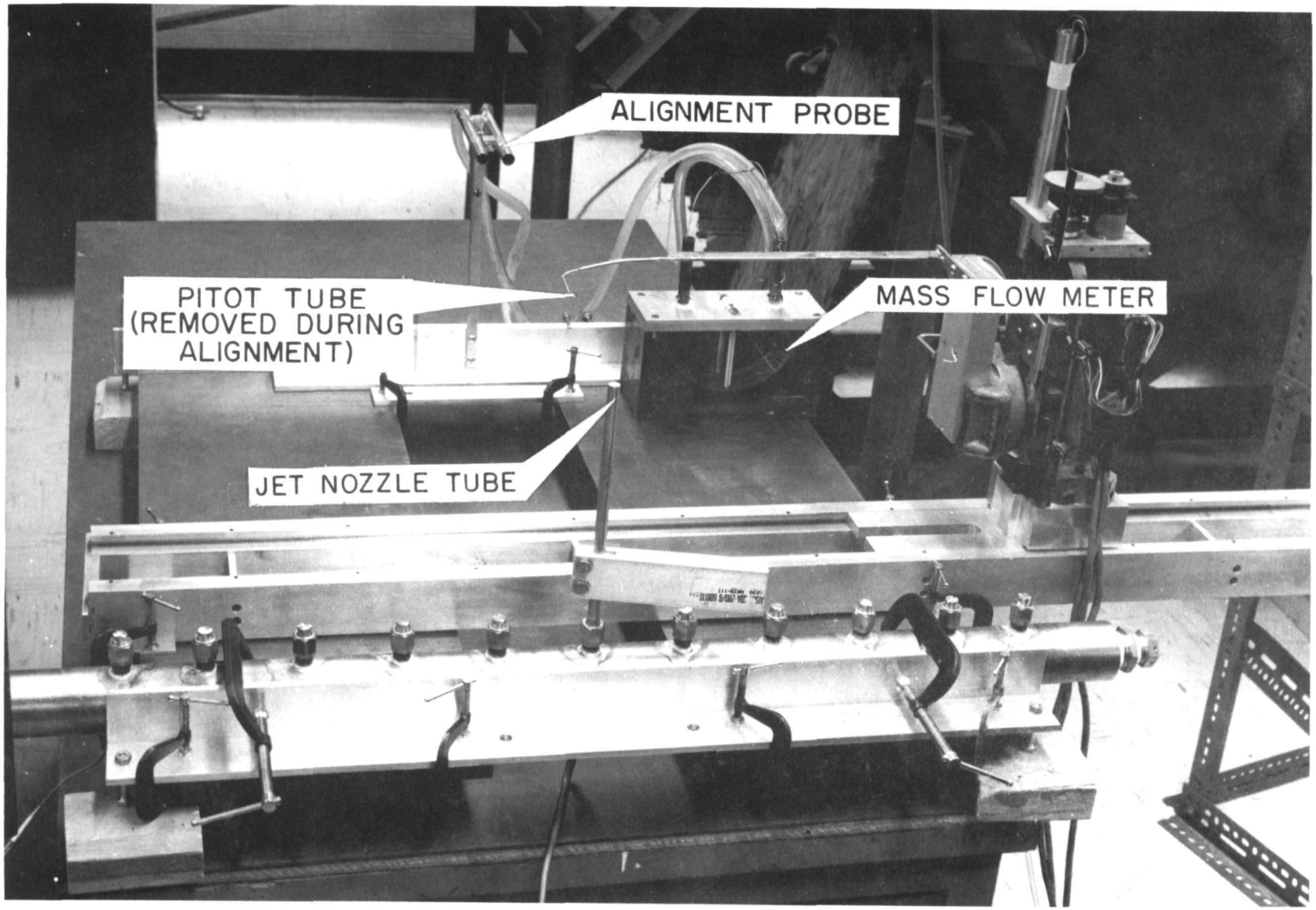

Figure 9. Photo of the jet nozzle alignment jig.

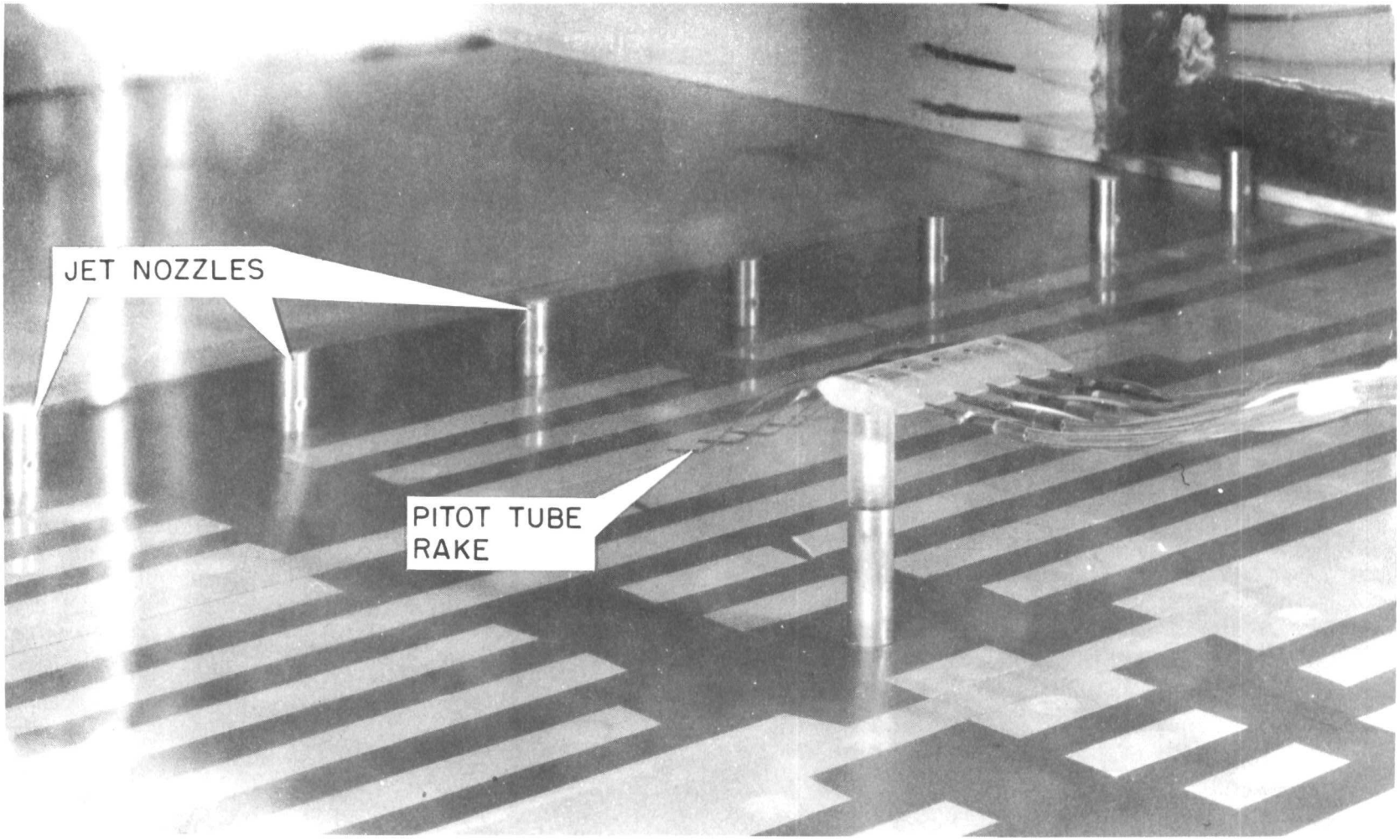

Figure 10. Photo showing the jet nozzles and the array of pitot tubes in the wind tunnel.

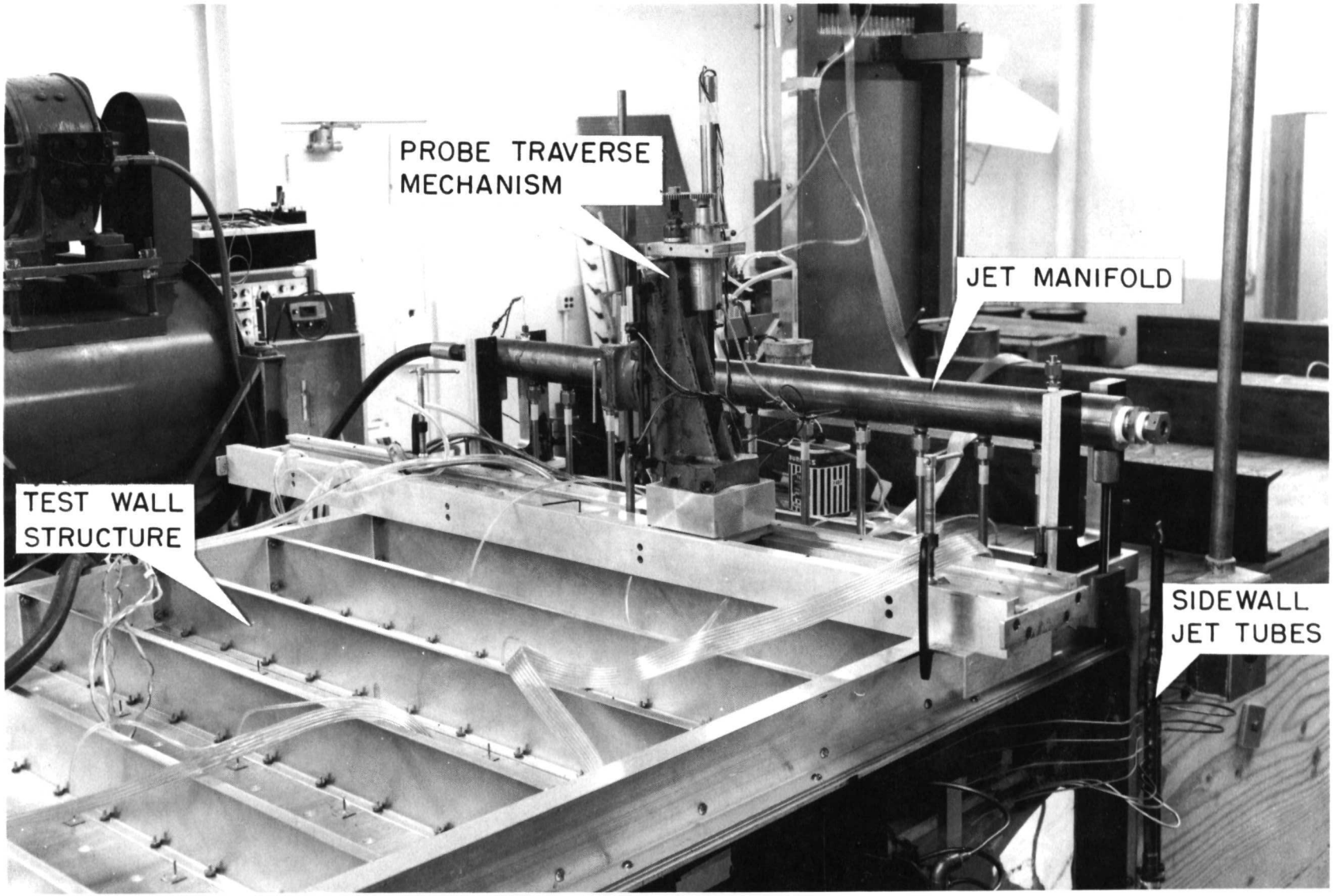

Figure 11. Photo of the top of the wind tunnel.

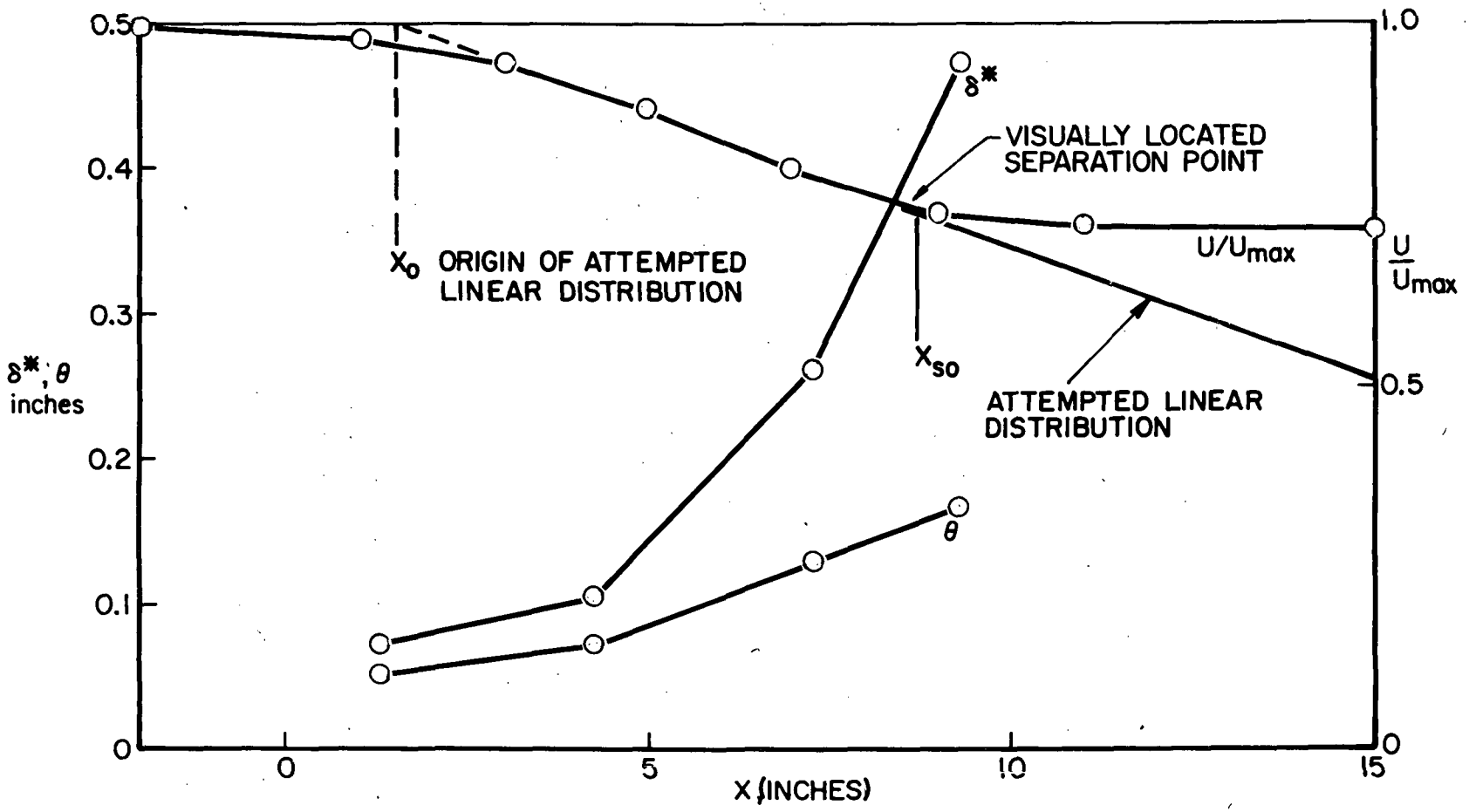

Figure 12. Distributions of free-stream velocity, Θ, and δ* in the large nozzle spacing case without blowing.

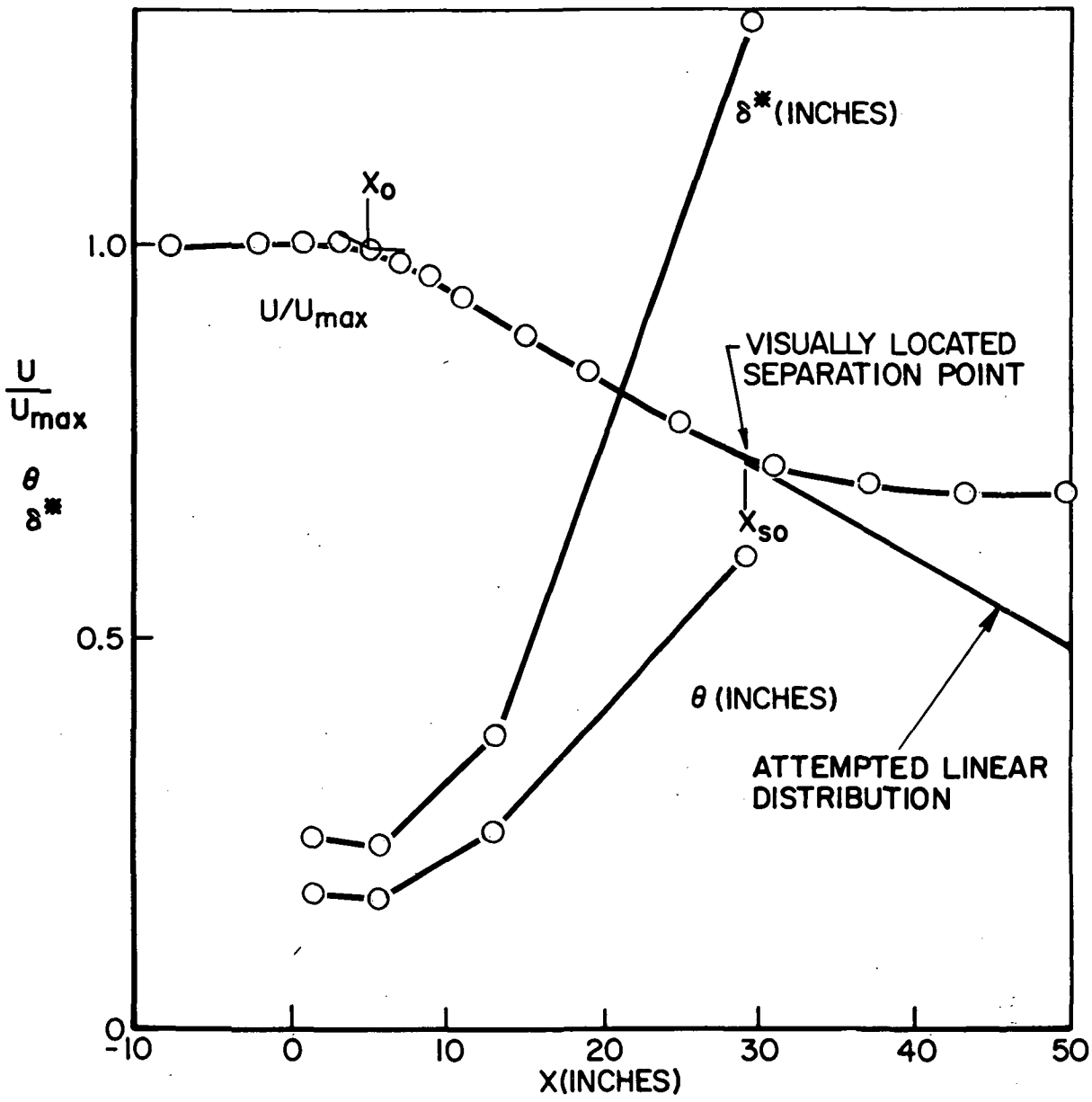

Figure 13. Distributions of free-stream velocity, Θ, and δ* in the small nozzle spacing case without blowing.

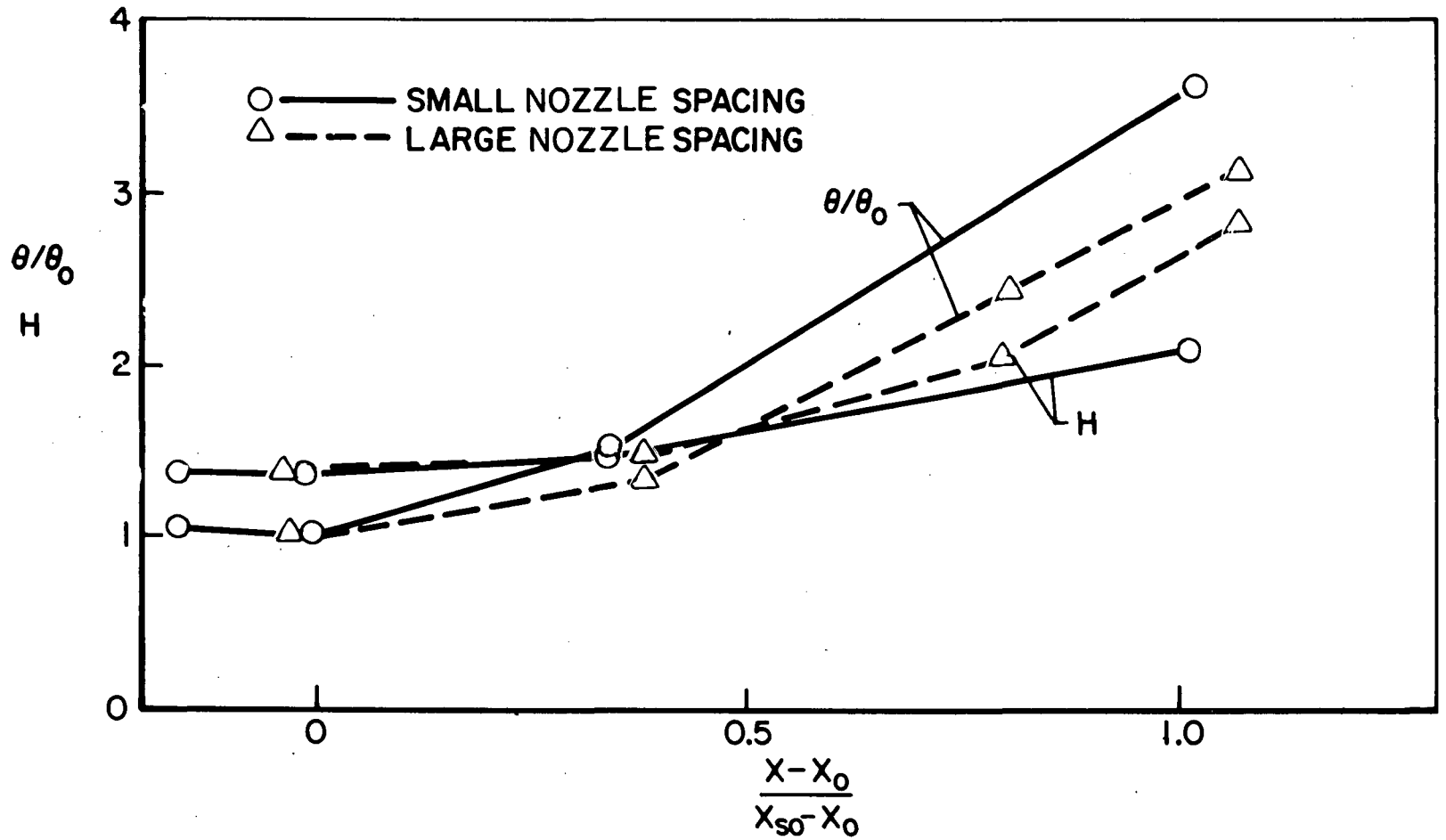

Figure 14. Dimensionless distributions of Θ/Θ_o and H in the no blowing cases.

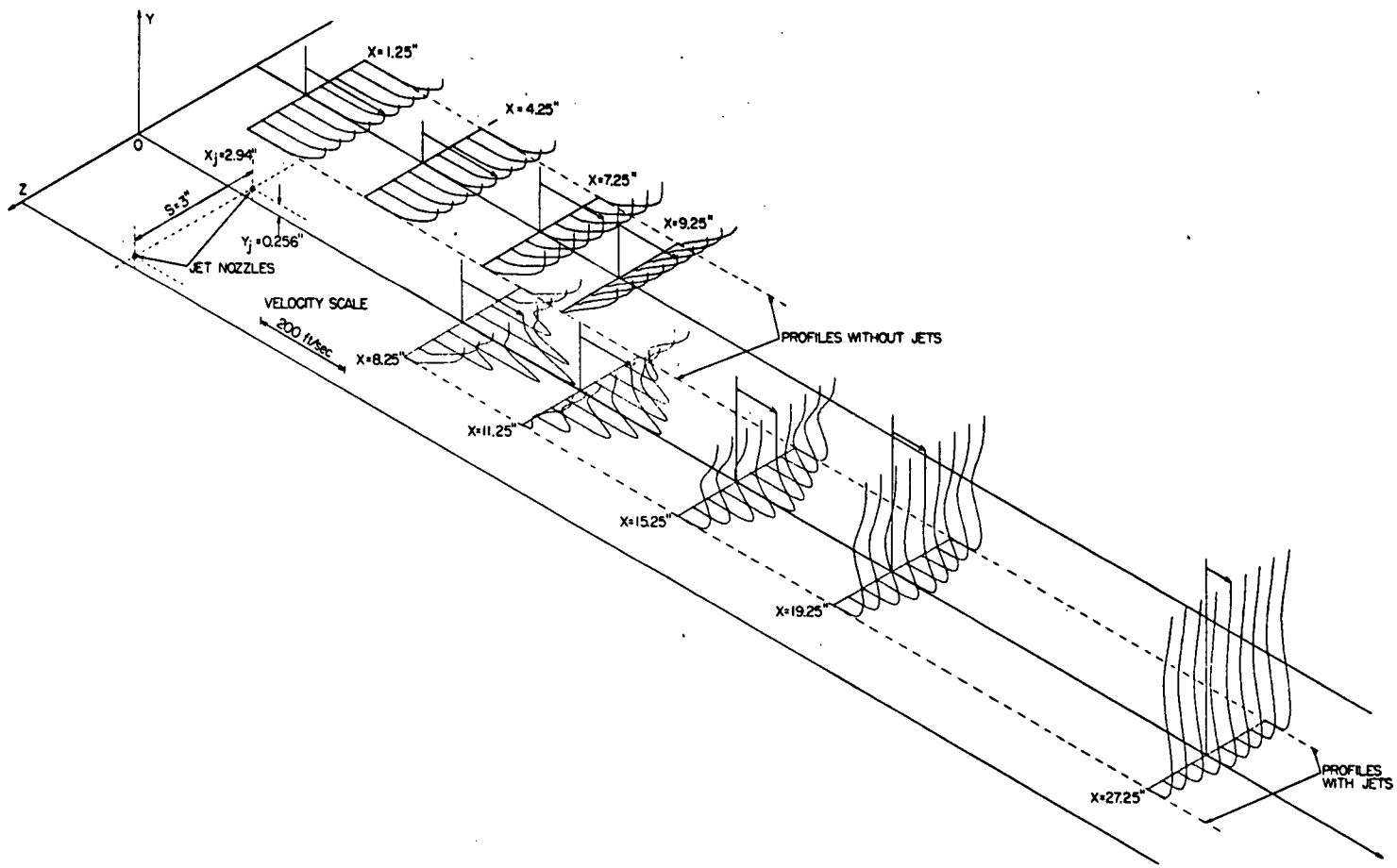

Figure 15. Isometric view of measured mean velocity profiles in the large nozzle spacing case with the flared nozzles.

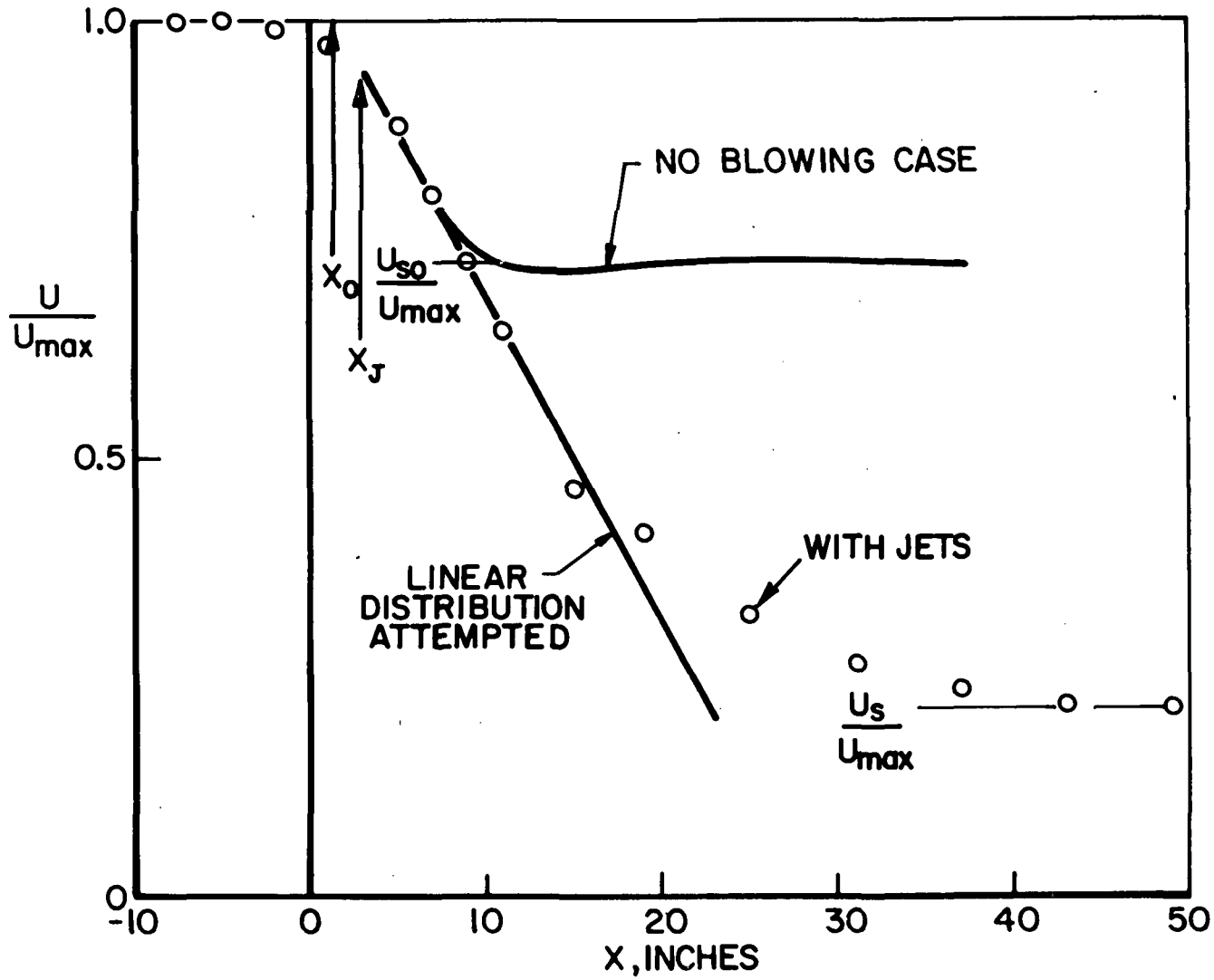

Figure 16a. Distribution of U versus x for the case with $y_j/S = 0.085$, $x_j = 2.91''$, $M_o = 1.74$. (The same case shown in Fig. 15)

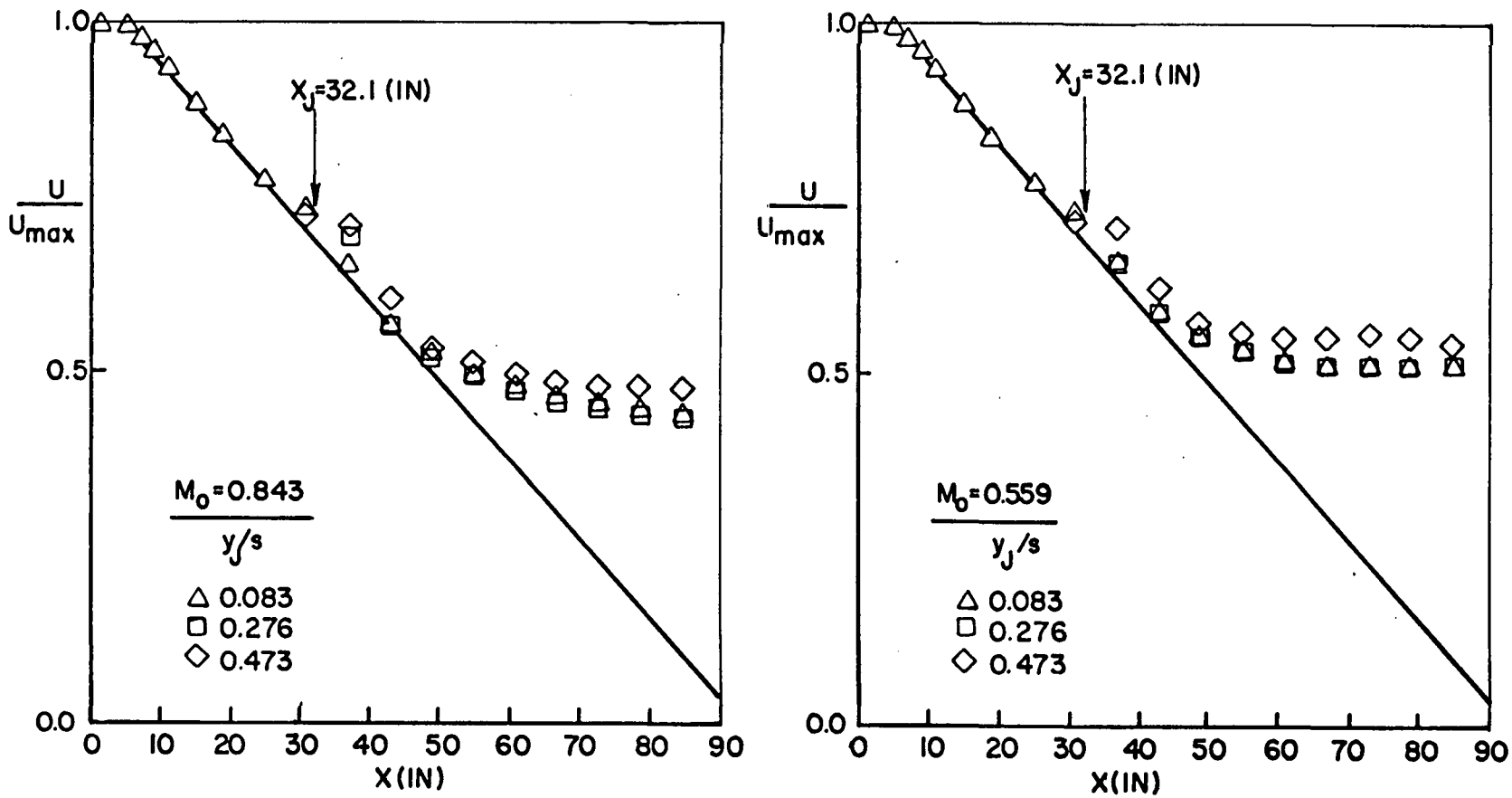

Figures 16b and 16c. Free-stream velocity distribution versus x.

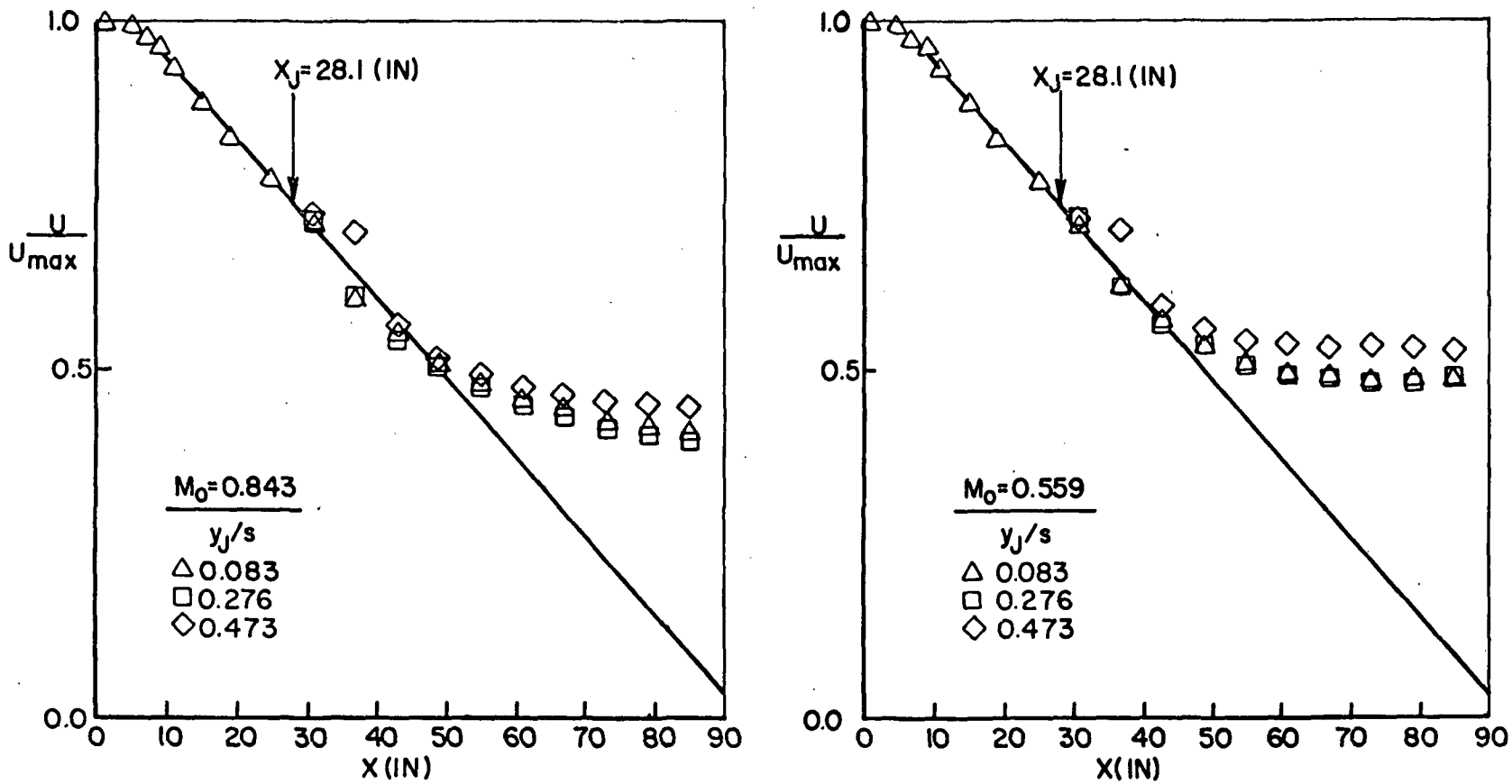

Figures 16d and 16e. Free-stream velocity distribution versus x.

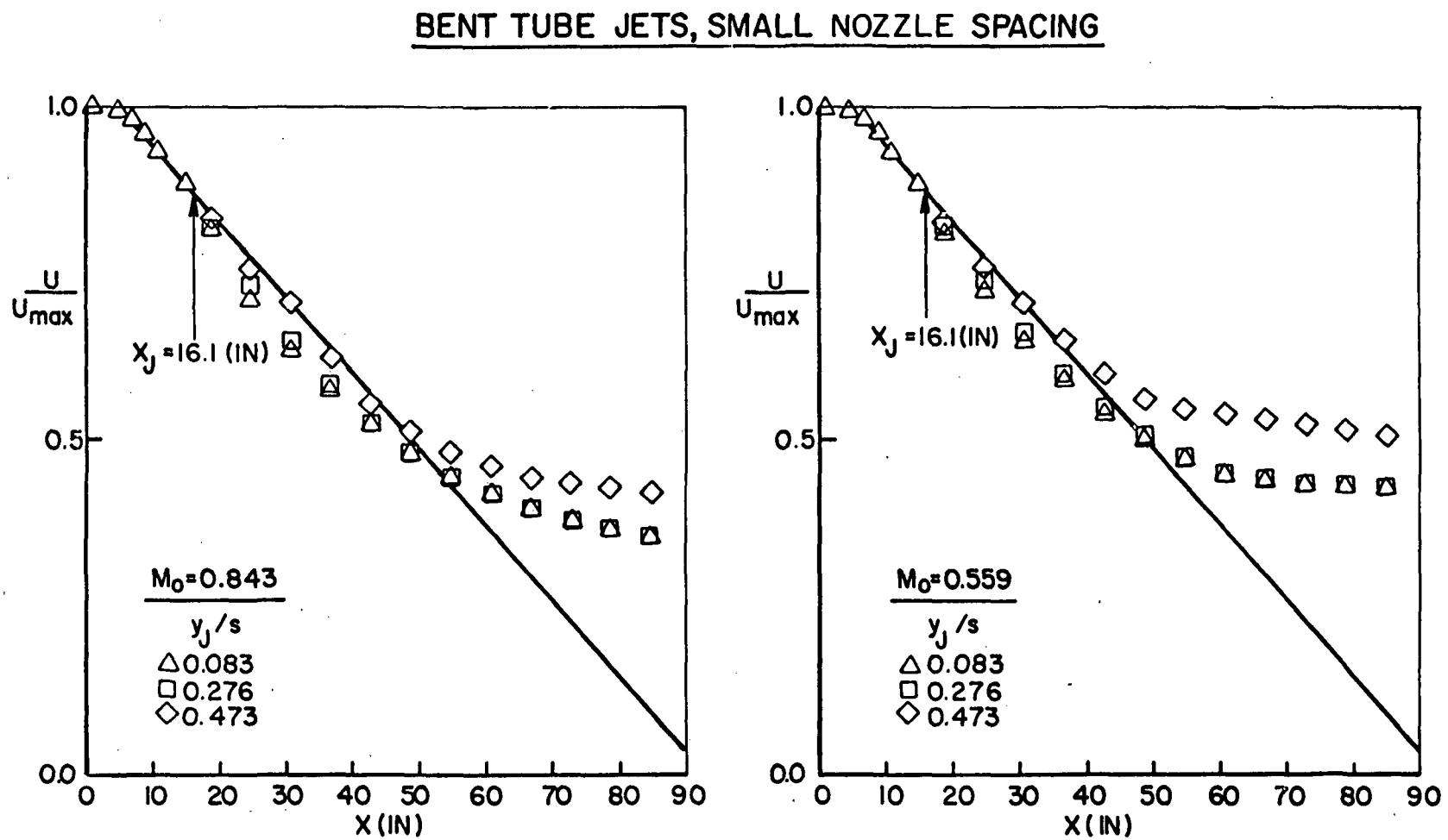

Figures 16f and 16g. Free-stream velocity distribution versus x.

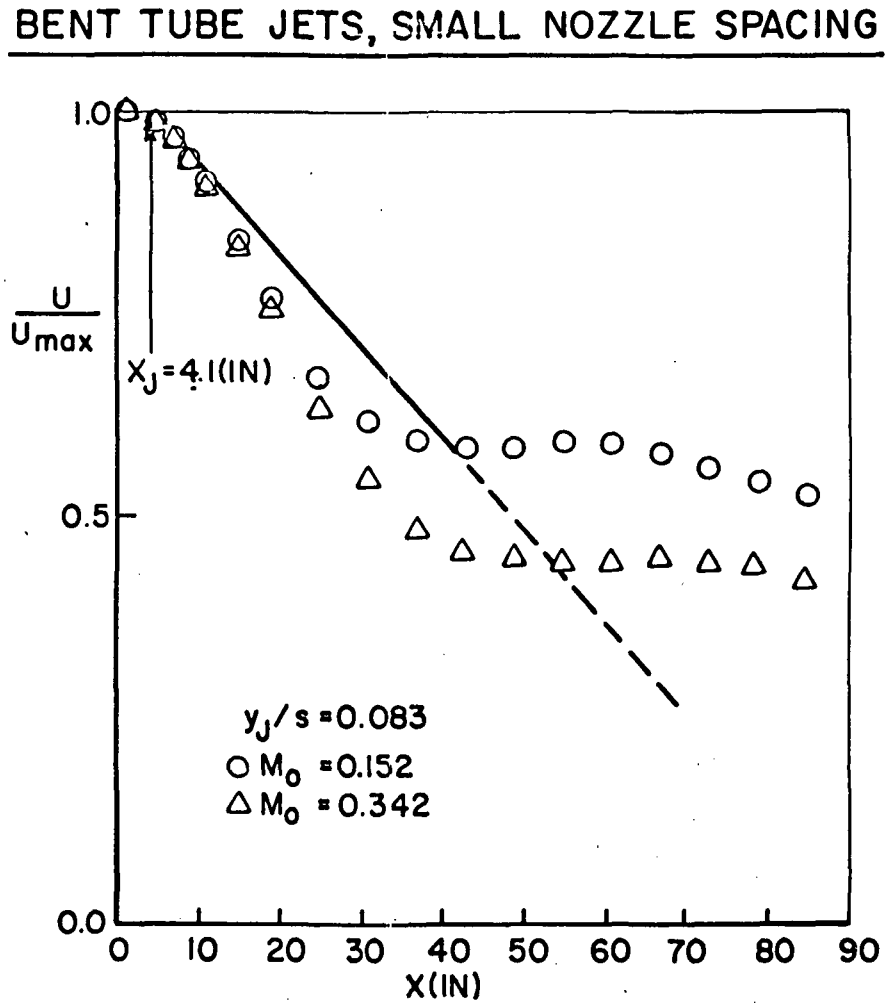

Figure 16h. Free-stream velocity distribution versus x.

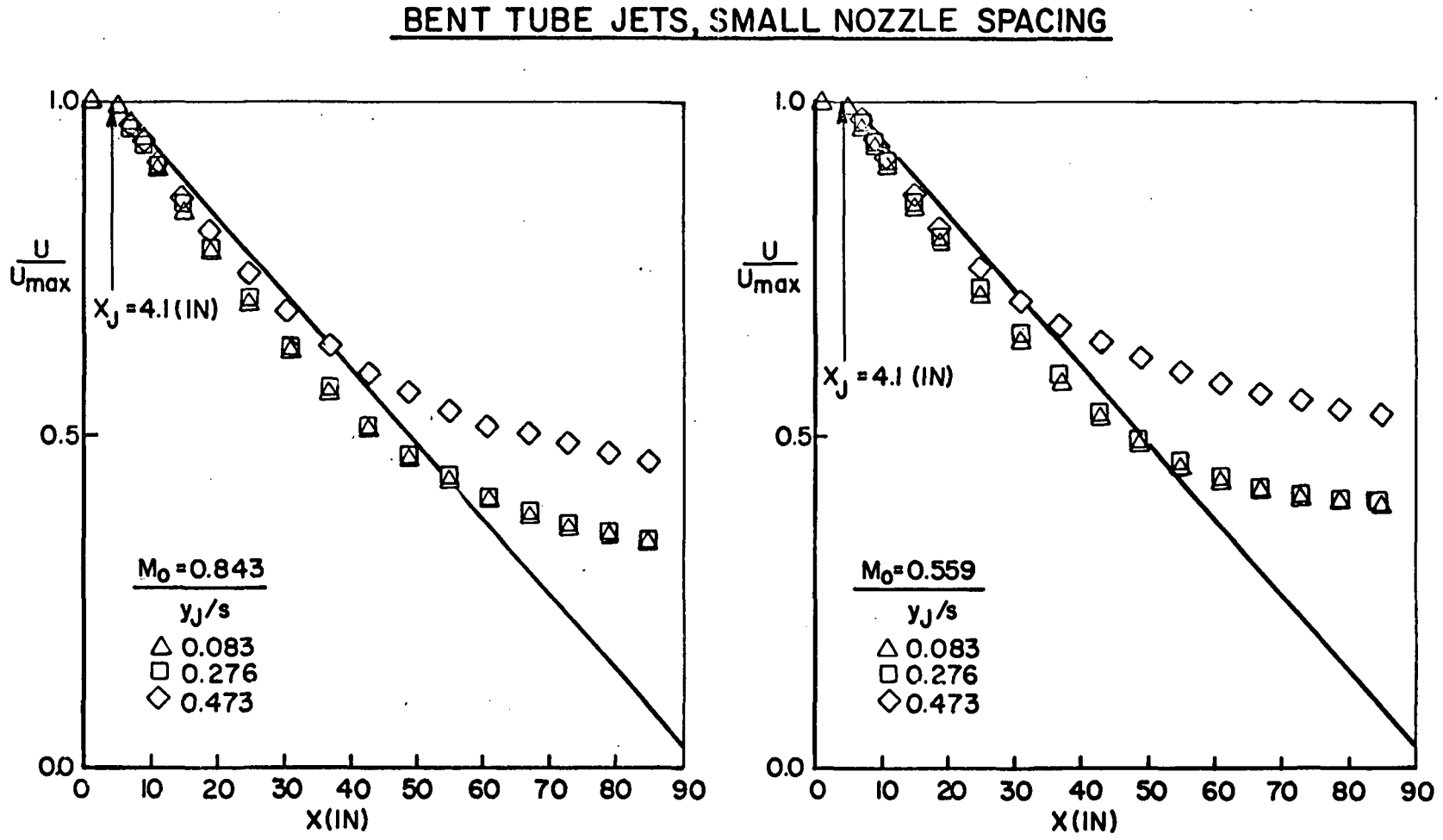

Figures 16i and 16j. Free-stream velocity distribution versus x.

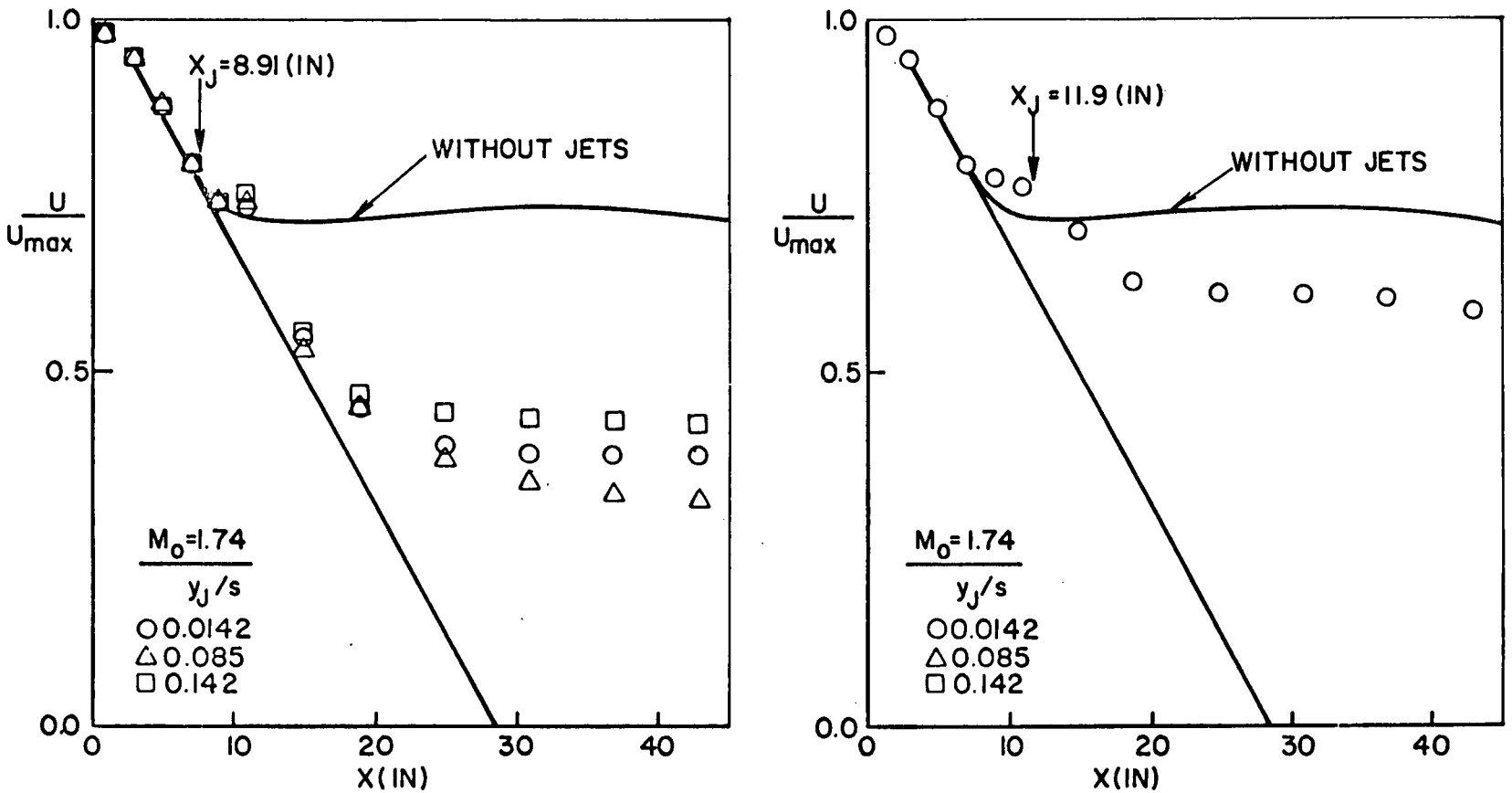

Figures 16k and 16ℓ. Free-stream velocity distribution versus x.

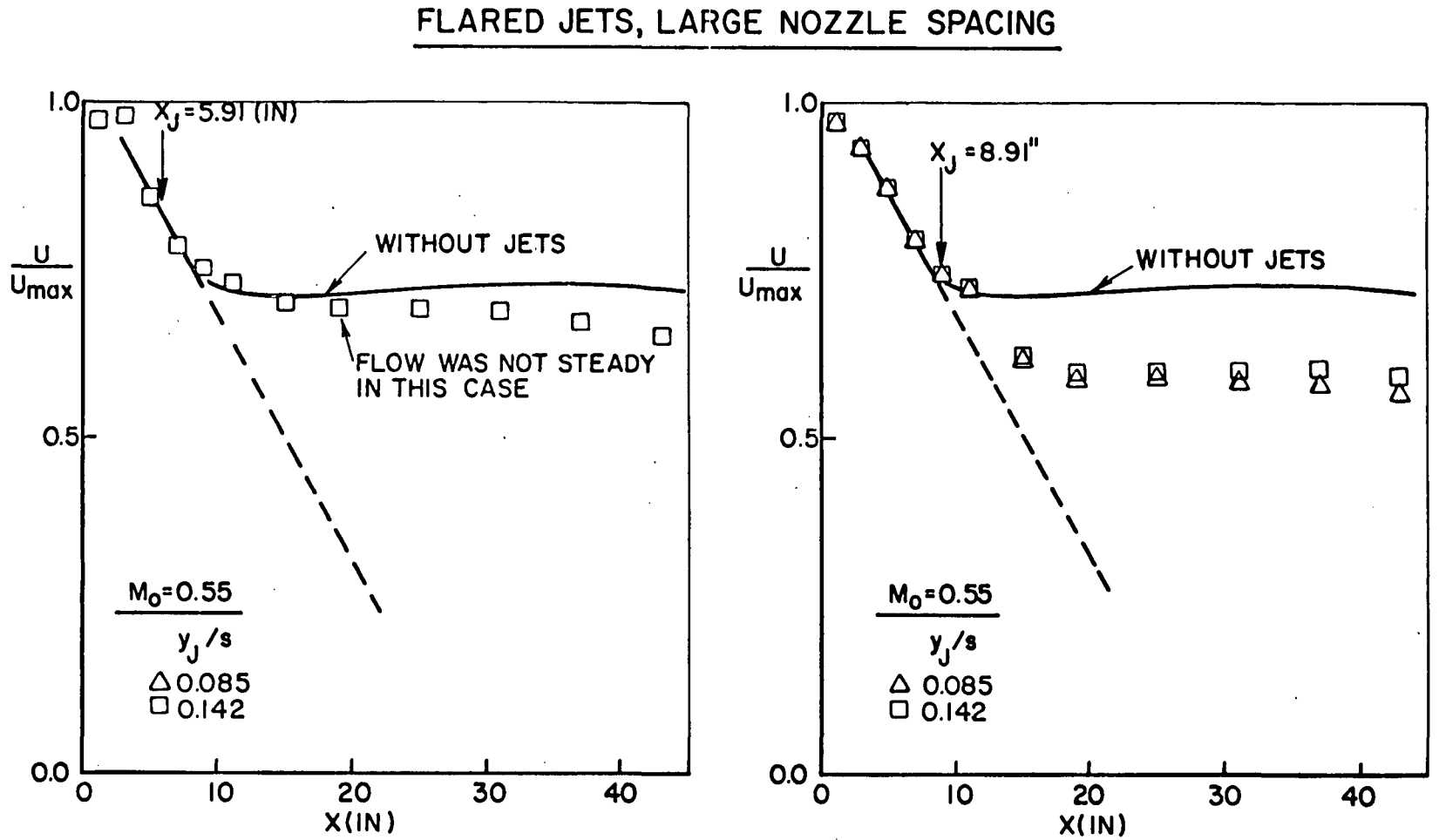

Figures 16m and 16n. Free-stream velocity distribution versus x.

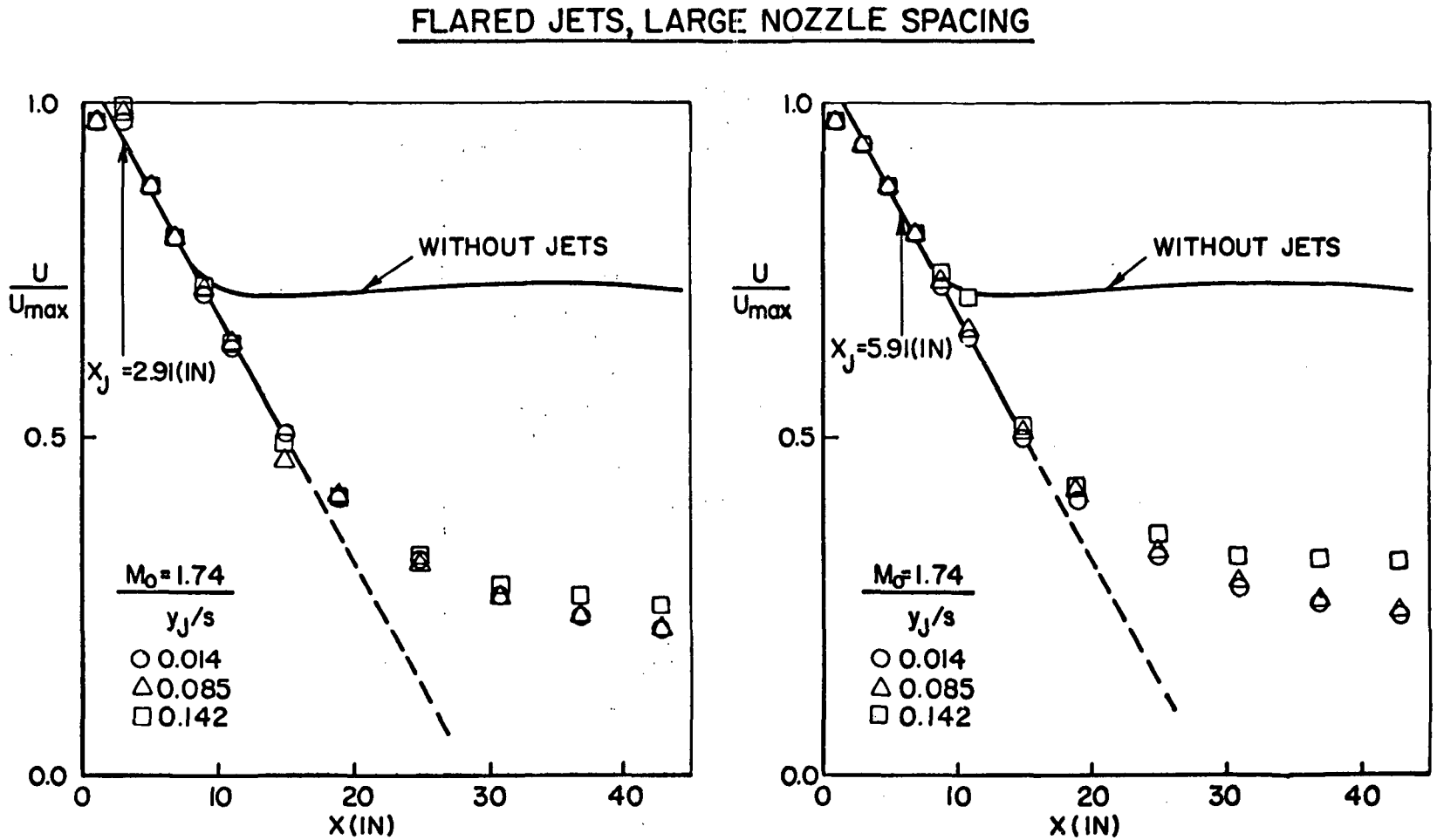

Figures 16o and 16p. Free-stream velocity distribution versus x.

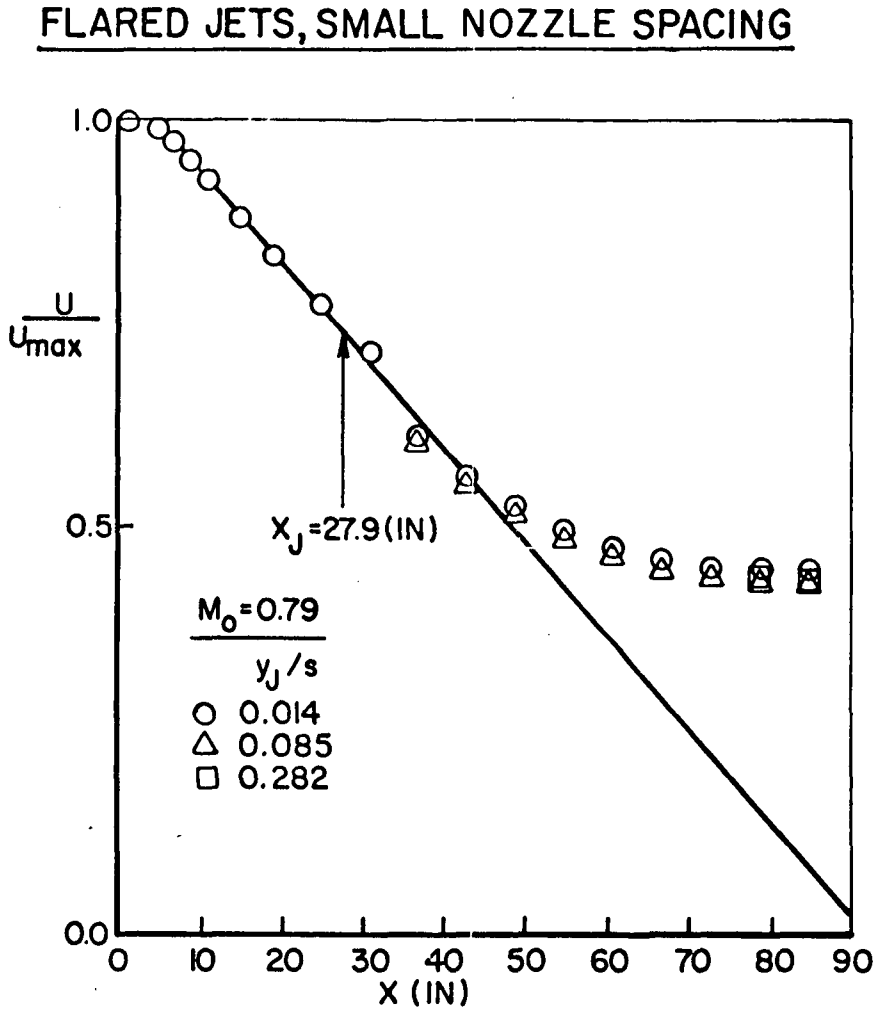

Figure 16q. Free-stream velocity distribution versus x.

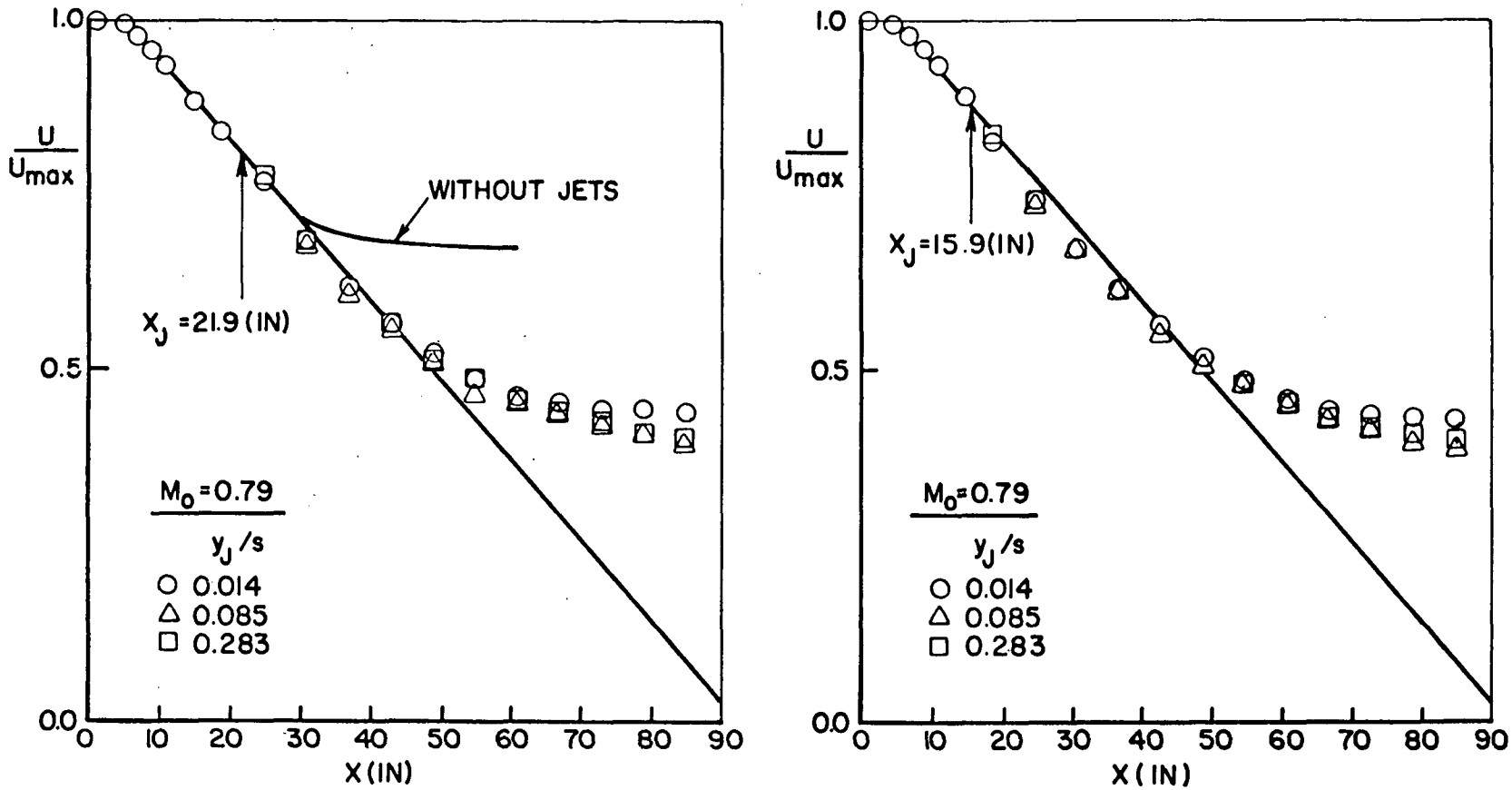

Figures 16r and 16s. Free-stream velocity distribution versus x.

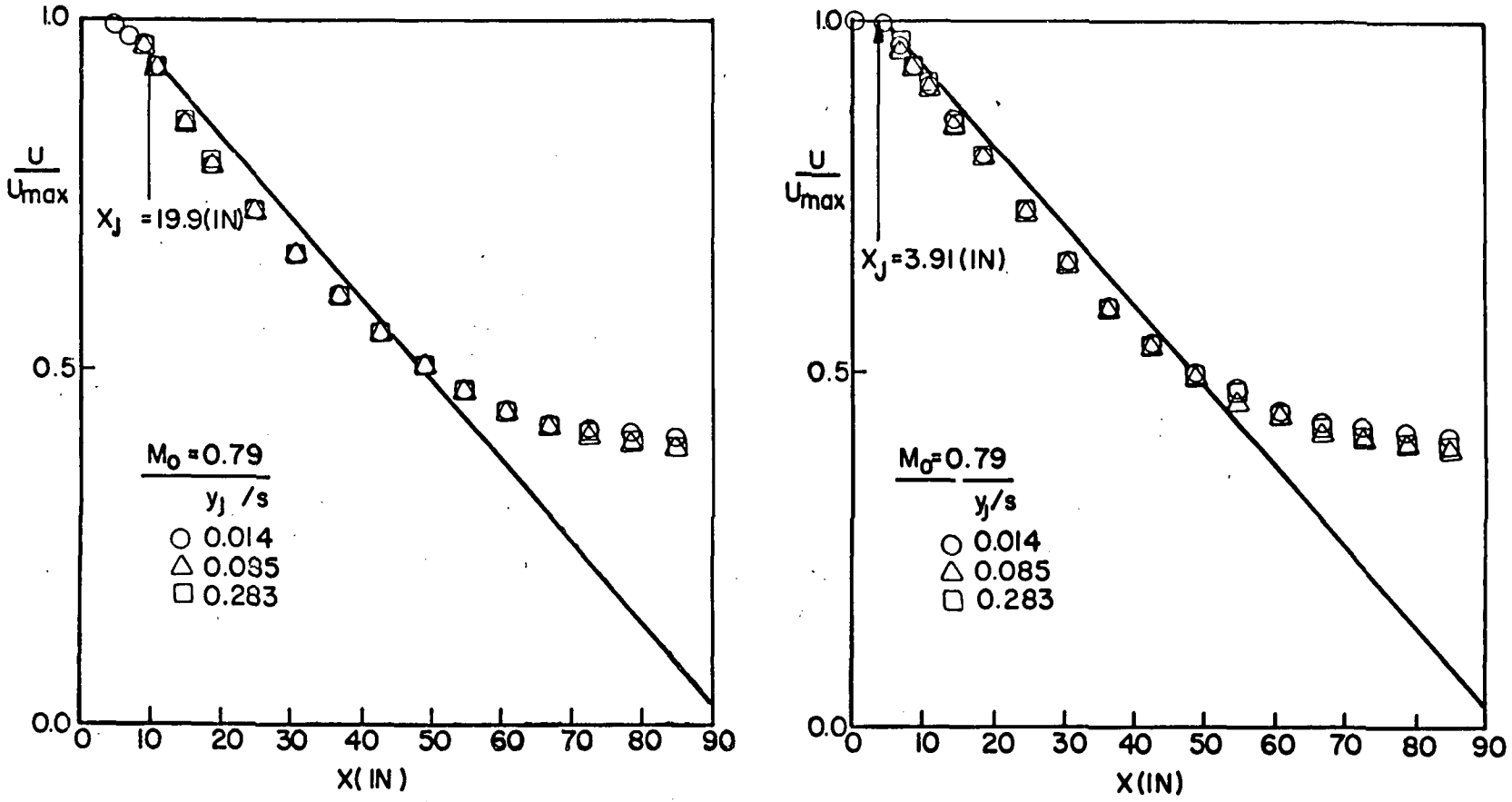

Figures 16t and 16u. Free-stream velocity distribution versus x.

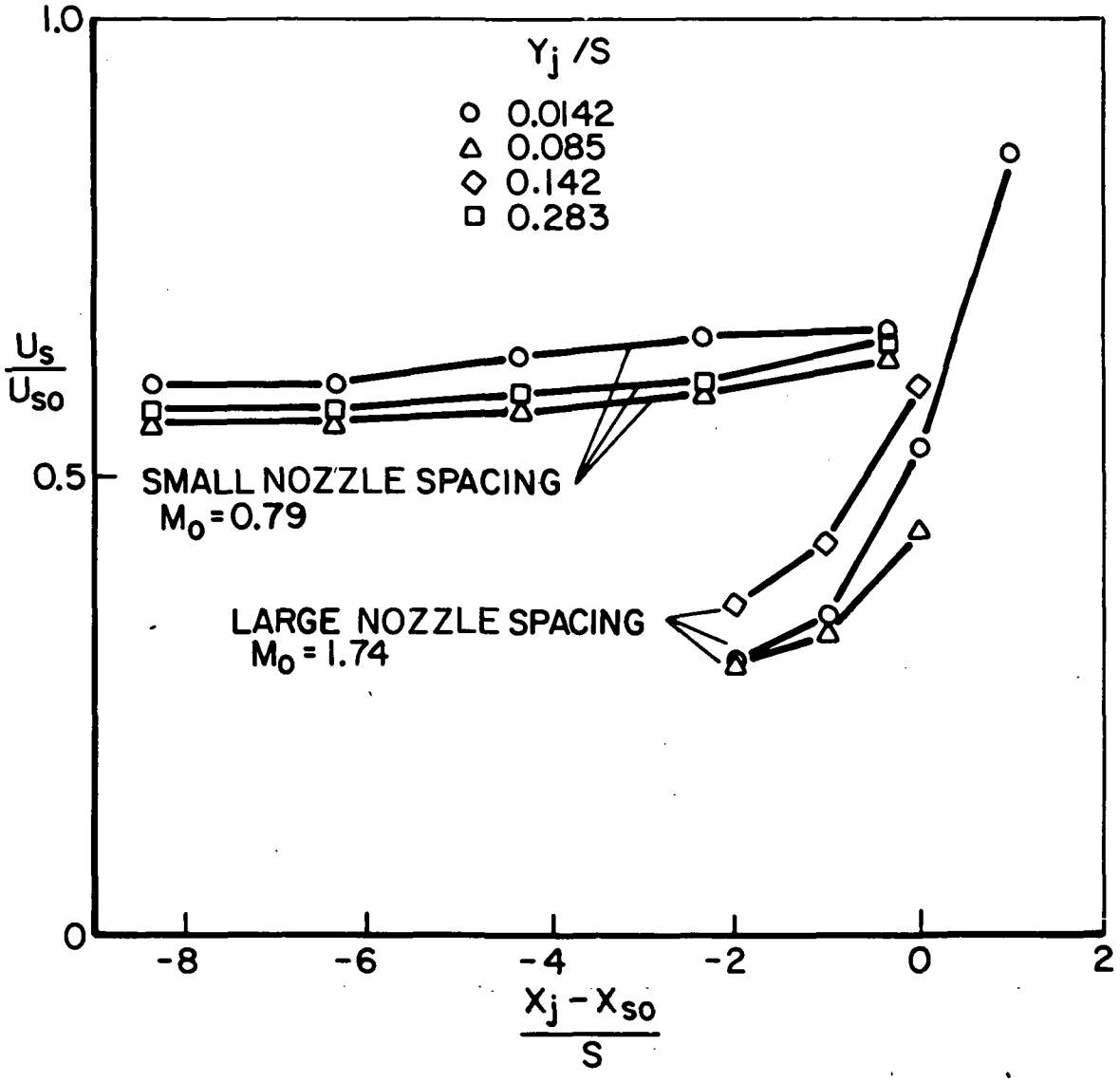

Figure 17. Plot showing the effect of nozzle location in the flared nozzle cases.

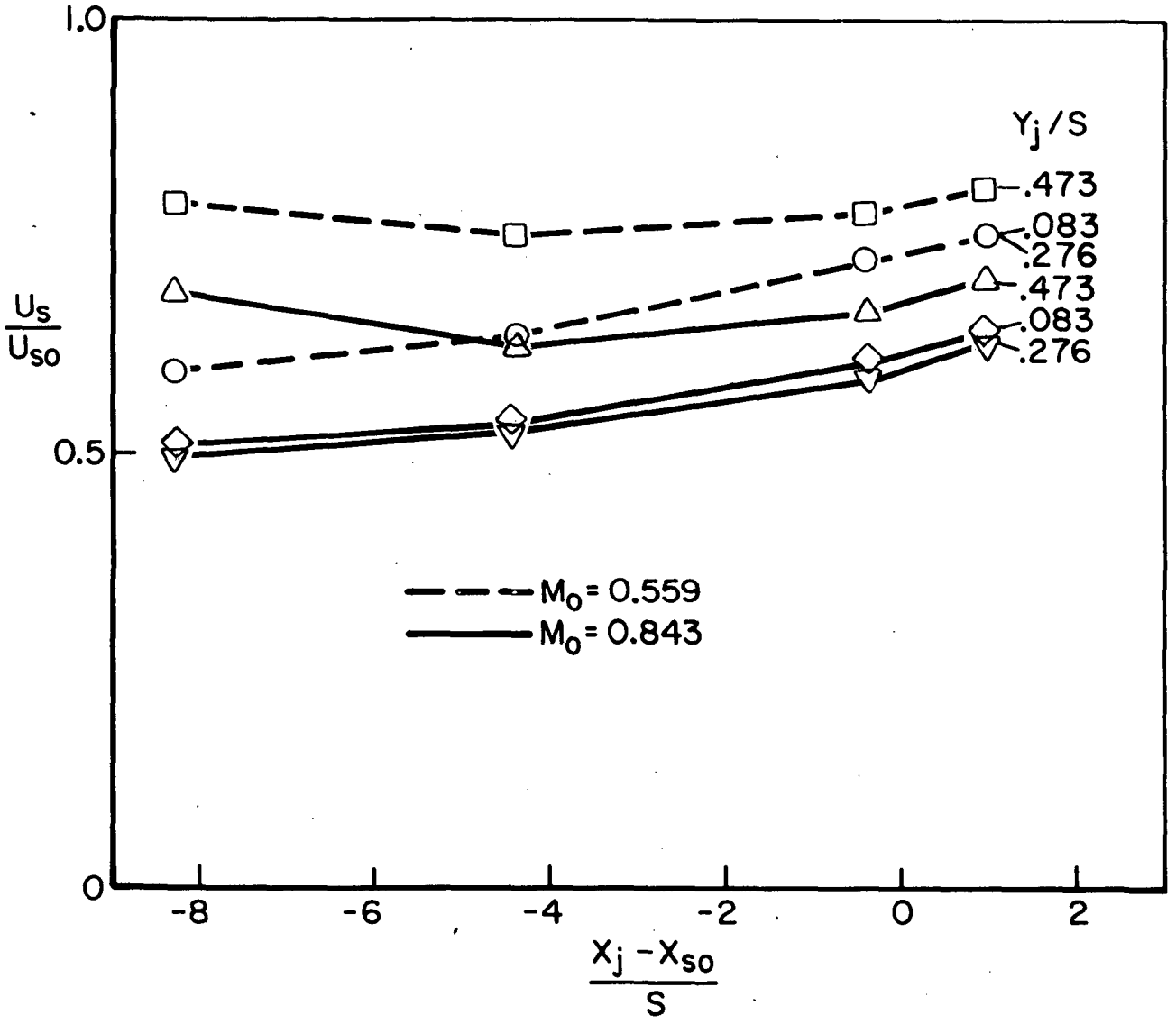

Figure 18. Plot showing the effect of nozzle location in the bent tube nozzle cases.

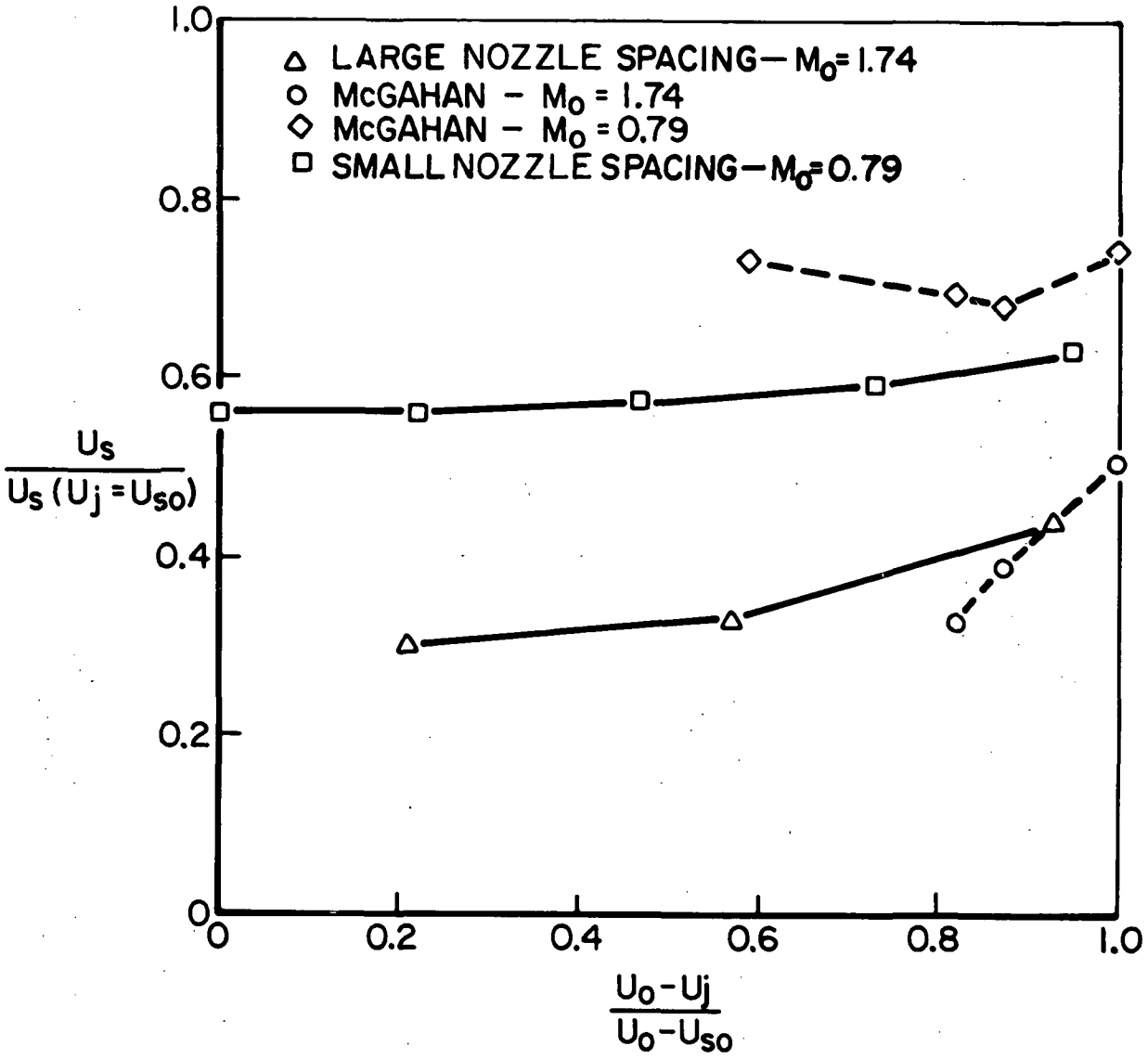

Figure 19. Dimensionless plot showing the effect of nozzle axial location, comparing the flared nozzles at y_j/S = 0.085 with McGahan's two-dimensional data.

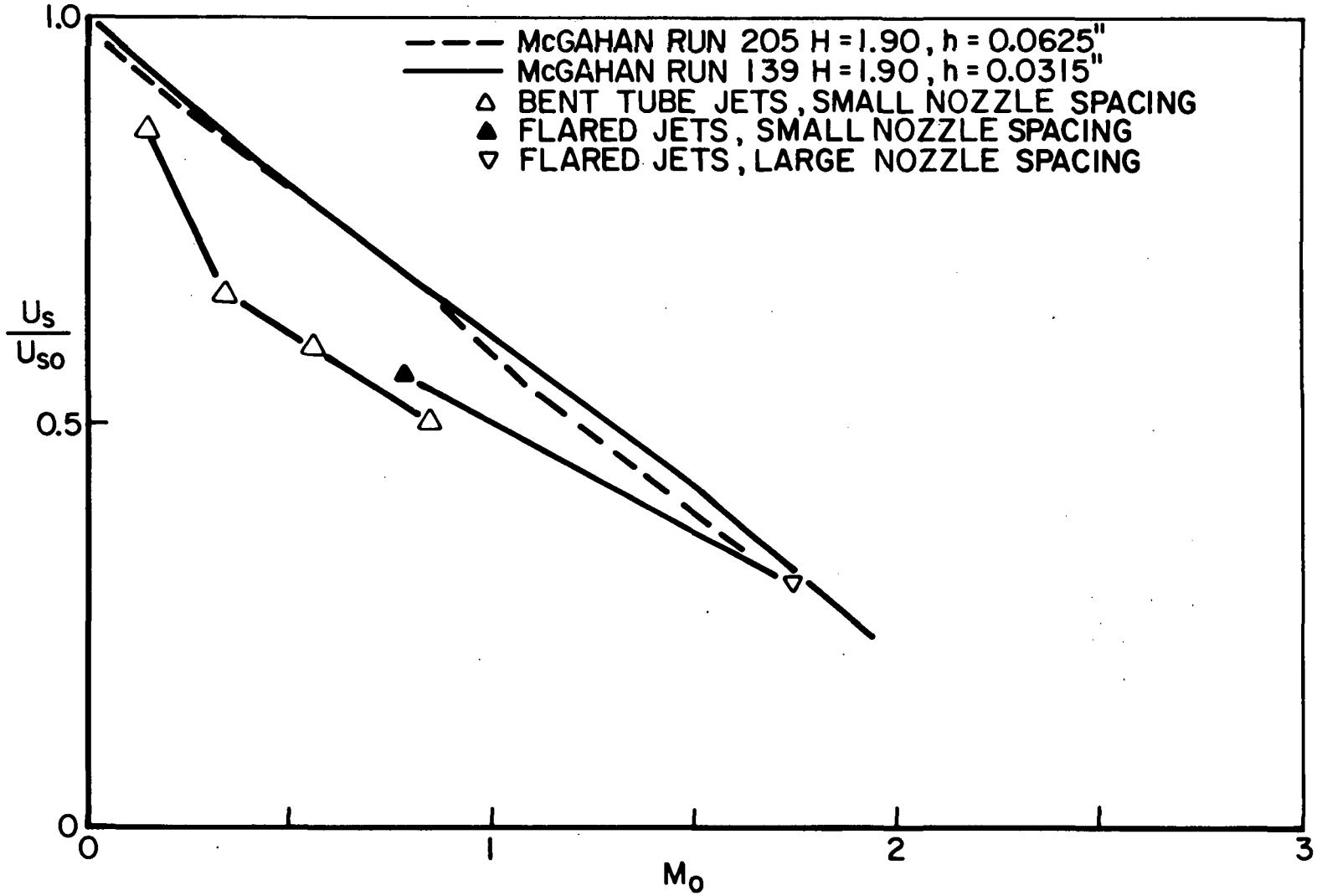

Figure 20. Correlation with M_o comparing discrete jets at their most advantageous locations with a two-dimensional slot.

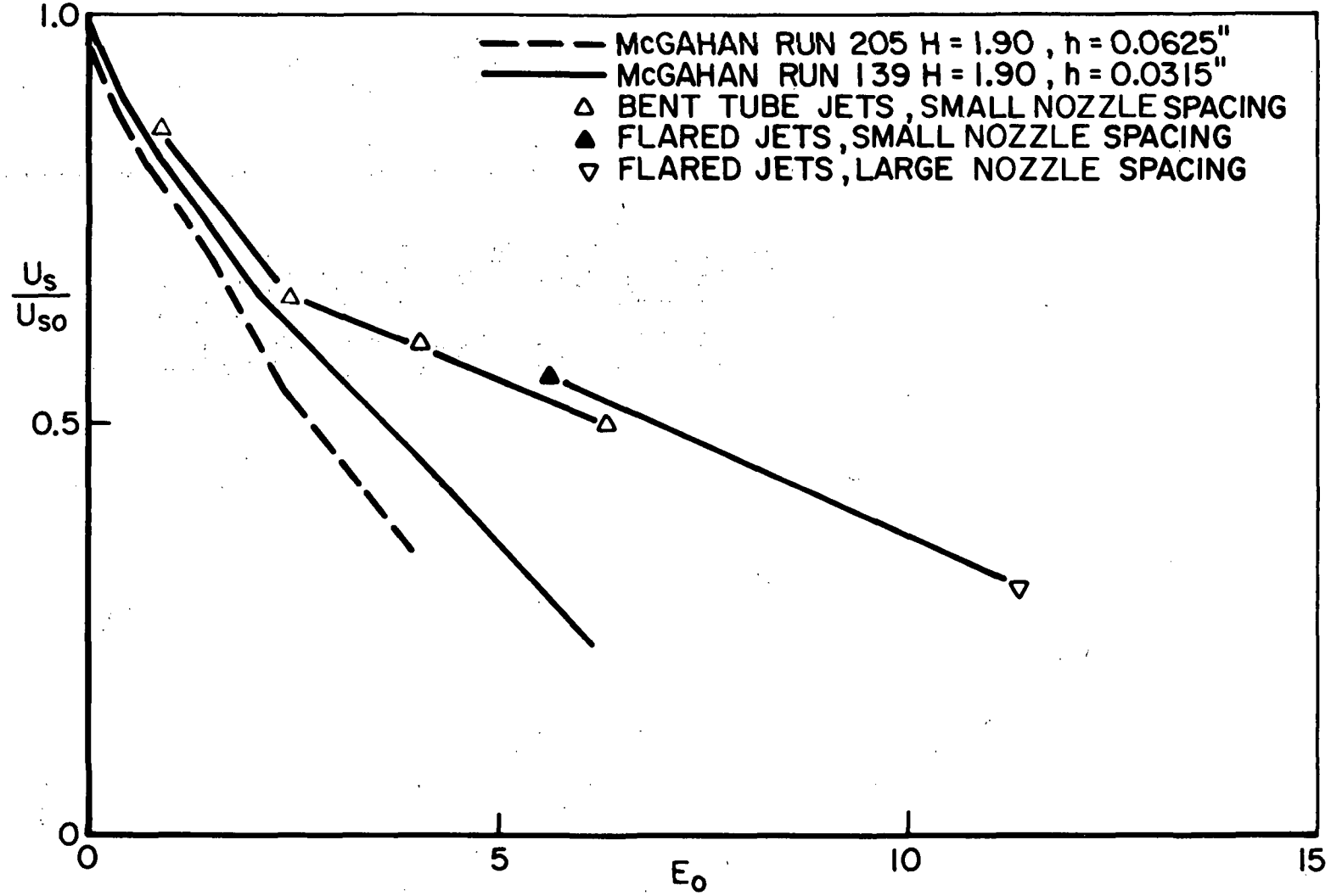

Figure 21. Correlation with energy parameter, E_o, comparing discrete jets at their most advantageous locations with a two-dimensional slot.

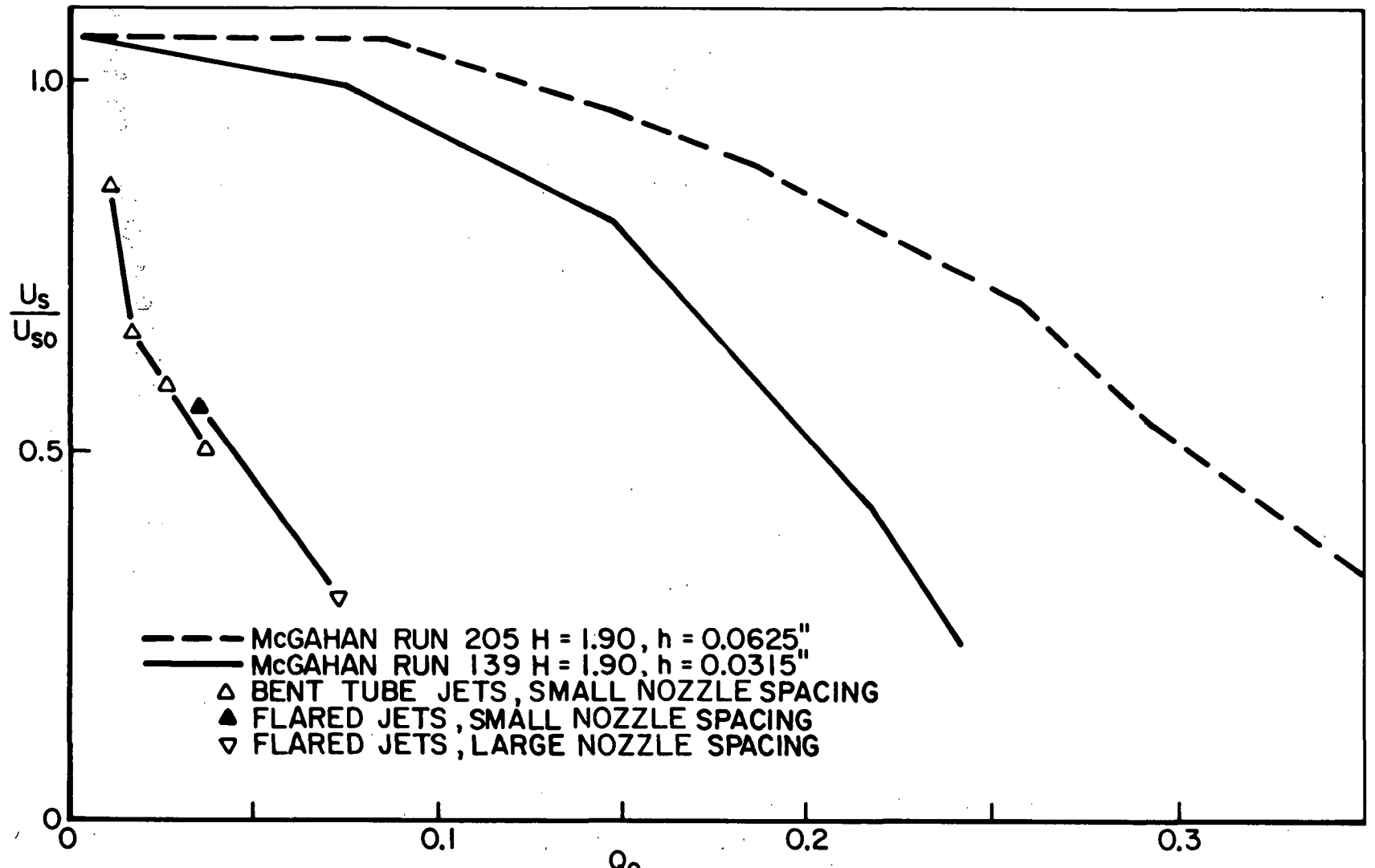

Figure 22. Correlation with mass flux parameter, Q_o, comparing discrete jets at their most advantageous locations with a two-dimensional slot.

Page Intentionally Left Blank

NATIONAL AERONAUTICS AND SPACE ADMINISTRATION
WASHINGTON, D.C. 20546

OFFICIAL BUSINESS
PENALTY FOR PRIVATE USE $300

SPECIAL FOURTH-CLASS RATE BOOK

POSTAGE AND FEES PAID
NATIONAL AERONAUTICS AND SPACE ADMINISTRATION
451

U.S.MAIL

POSTMASTER: If Undeliverable (Section 158 Postal Manual) Do Not Return

"The aeronautical and space activities of the United States shall be conducted so as to contribute . . . to the expansion of human knowledge of phenomena in the atmosphere and space. The Administration shall provide for the widest practicable and appropriate dissemination of information concerning its activities and the results thereof."

—NATIONAL AERONAUTICS AND SPACE ACT OF 1958

NASA SCIENTIFIC AND TECHNICAL PUBLICATIONS

TECHNICAL REPORTS: Scientific and technical information considered important, complete, and a lasting contribution to existing knowledge.

TECHNICAL NOTES: Information less broad in scope but nevertheless of importance as a contribution to existing knowledge.

TECHNICAL MEMORANDUMS: Information receiving limited distribution because of preliminary data, security classification, or other reasons. Also includes conference proceedings with either limited or unlimited distribution.

CONTRACTOR REPORTS: Scientific and technical information generated under a NASA contract or grant and considered an important contribution to existing knowledge.

TECHNICAL TRANSLATIONS: Information published in a foreign language considered to merit NASA distribution in English.

SPECIAL PUBLICATIONS: Information derived from or of value to NASA activities. Publications include final reports of major projects, monographs, data compilations, handbooks, sourcebooks, and special bibliographies.

TECHNOLOGY UTILIZATION PUBLICATIONS: Information on technology used by NASA that may be of particular interest in commercial and other non-aerospace applications. Publications include Tech Briefs, Technology Utilization Reports and Technology Surveys.

Details on the availability of these publications may be obtained from:

SCIENTIFIC AND TECHNICAL INFORMATION OFFICE

NATIONAL AERONAUTICS AND SPACE ADMINISTRATION

Washington, D.C. 20546